CHAPTER III

RESULTS AND DISCUSSION

3.1. Introduction

An experimental set-up was constructed to heat a material layer sample uni-directionally from the sample surface, to study heat transfer to and within the layer. Large differentials between the sample surface temperature and bed temperatures, at increasing depth from the sample surface, show conduction heat transfer control within the layer of material. Increased reduction extent for decreased material layer thickness would also confirm conduction heat transfer control within the material layer. Large temperature differentials between the sample surface and the furnace heating surfaces would indicate radiation heat transfer control. Also, increased reduction extent achieved for increased heat transfer rate would confirm radiation heat transfer control. These ideas were tested experimentally, and the results are reported below.

Mixtures of coal and ore were reacted at heating zone 1 temperatures of 1300°C, 1400°C and 1500°C to measure the extent of reaction at increased heat input into the sample. Sishen fines and Eikeboom coal of -850 +425 µm were used as input materials for the bulk of the experiments. A molar ratio of fixed carbon to reducible oxygen in ore of 0.97 was used. The input material chemical compositions are shown in **Appendix IV**. To test the effect of different particle sizes, ore and coal fractions of -425 +300 µm and -2000 +1400 µm were also used. The material layer thickness of 40 mm was used as basis, and a series of 16 mm material layer thickness was tested for comparison. To determine the devolatilisation components of the coal, the ore portion in the sample mixture was replaced by alumina particles of the same particle size as the ore. The coal-alumina samples were then reacted to complete devolatilisation. The radiation network calculation from Chapter II was used to calculate radiation heat transfer to the sample surface at one second intervals. The reacted samples were sectioned into three parts, as shown in Chapter II, and analysed for reduction extent and carbon content.

The product gas was analysed by mass spectrometer. As an example the data set of sample temperatures, furnace heating zone temperatures and product gas analyses measured in each experiment is shown in **Fig. 24** for the 40 mm layer thickness sample, of coal-ore mixture, reacted for 15 minutes at 1400°C heating zone 1 temperature. Similar sets of data for all the samples reacted are shown in **Appendix VIII** in graphical form. The iron balance for the samples was calculated and the

*Reducible oxygen is the oxygen bound to the total Fe analysed in the iron ore, expressed as Fe_2O_3

ratio of iron into the sample to iron out of the reacted sample varied from 0.99 to 1.08. These values are summarised in **Appendix XI**, as are sample analyses and total product gas analyses.

The total mass loss according to the product gas analyses was compared to the sample mass weighed after the sample was split into three sections, and these measurements corrected for fiberboard crucible material carry over. The values are summarised in **Appendix XI**, and graphs are shown in **Appendix X**. In most instances the difference in mass loss as percentage of the mass loss calculated from the weighed sample mass of the reacted sample is within 30% of the sample mass loss calculated from the product gas analysis. The biggest difference of 100% was for the 40 mm sample layer with fine ore fraction reacted for 9 minutes at 3.13 g mass loss.

The mass of carbon reacted, as calculated from %C analyses of the reacted material, was similarly compared to that calculated from the product gas analyses. Graphs of mass carbon remaining as calculated from these two information sources are shown in graphs in **Appendix X**. The analysis uncertainty for total carbon analysis in the reacted ore-coal mixture, ±1.5%C as shown in **Fig. 14 (b)**, is indicated by error bars in the graphs. With the exception of the 16 mm sample layer reacted for 15 minutes the difference in mass carbon remaining in the reacted sample, expressed as percentage of the mass of carbon remaining as calculated from the reacted sample carbon analysis, is within 20% of the mass carbon remaining calculated from the product gas analysis. The 57% percentage difference for the 16 mm sample layer reacted for 15 minutes was 0.70 g carbon of 1.20 g carbon calculated from the carbon analysis on the reacted sample.

Similarly the mass oxygen released in the product gas analyses was compared to the mass oxygen reduced from the ore as calculated from the forms of Fe analyses. The uncertainty in the mass oxygen release calculation from the forms of Fe analyses is that the oxygen released from coal is not included in the calculation. This uncertainty is shown as error bars in the graphs in **Appendix X**. Without taking the error estimation into account the maximum difference in mass oxygen released form the sample, as percentage of the mass oxygen released as calculated from the forms of Fe analyses, is 78%. This percentage difference is 0.55 g oxygen of 0.70 g oxygen released into the product gas for a 16 mm sample layer reacted for 3 minutes, and 1.64 g oxygen of 2.09 g oxygen released into the product gas for a 40 mm sample layer with fine ore fraction reacted for 9 minutes.

The product gas analyses were used to calculate the CO/CO_2 ratios in the product gas. These values were compared to the equilibrium gas ratios for the FeO/Fe and the C/CO_2 equilibrium to indicate which reaction was more important in the reaction system. The %C and forms of Fe analyses in the reacted samples were used in reaction extent calculations.

Fig. 24: Temperatures and product gas analyses for 40 mm layer thickness of coal-ore mixture reacted at 1400°C for 15 minutes.

(a) Sample Temperatures

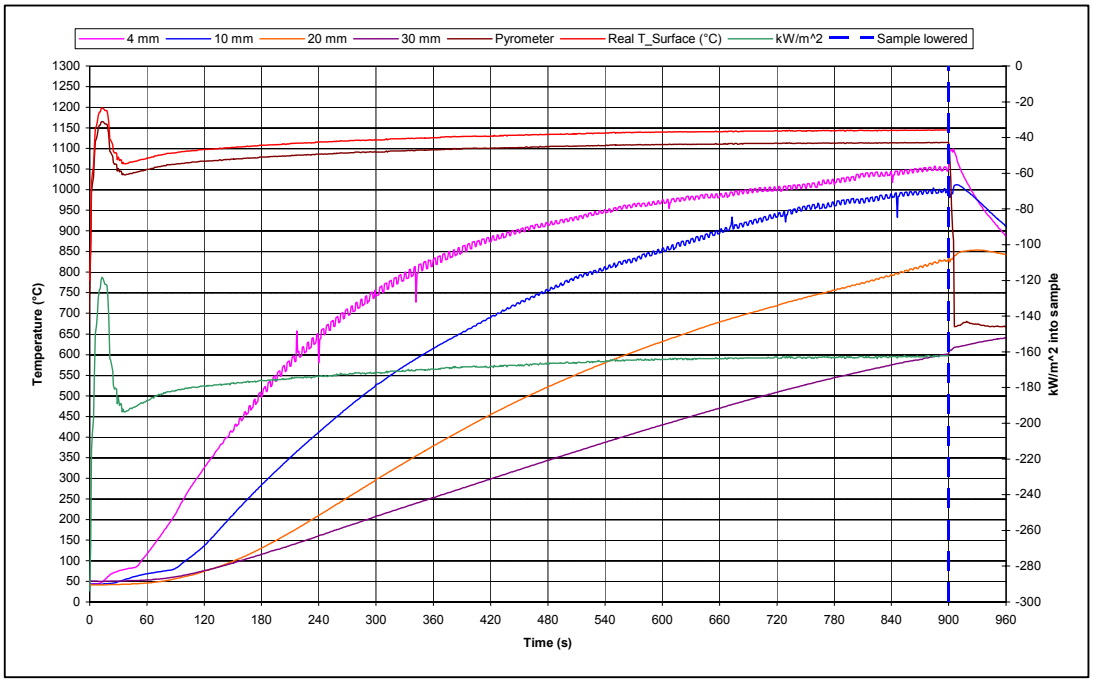

(b) Product gas analyses

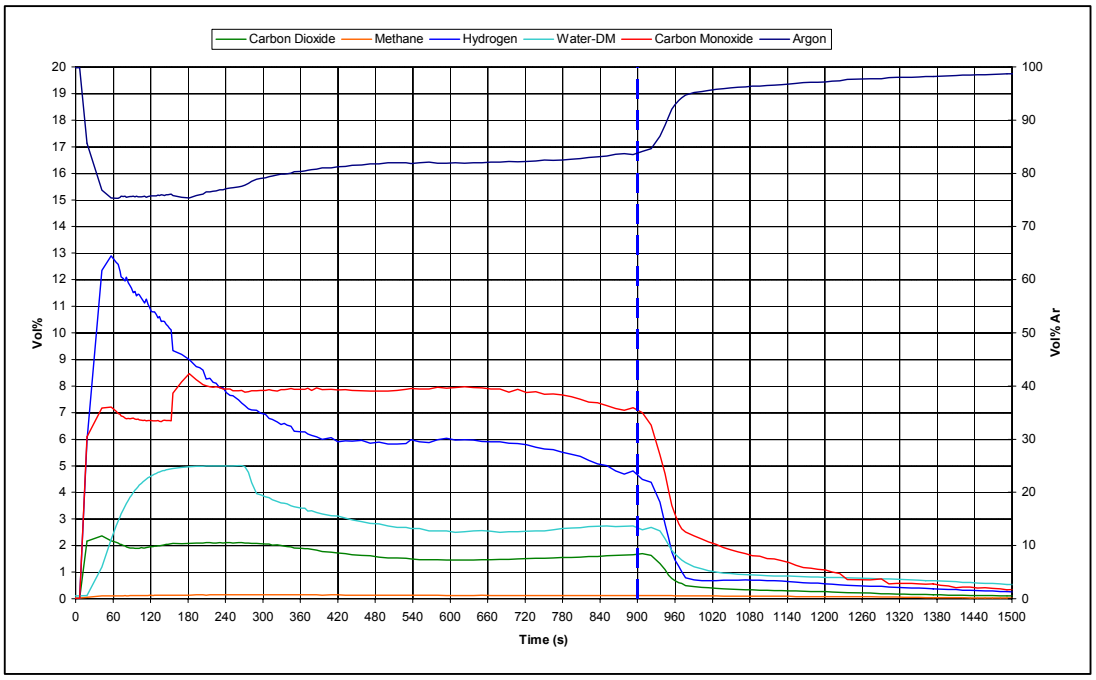

(c) Furnace heating zone temperatures

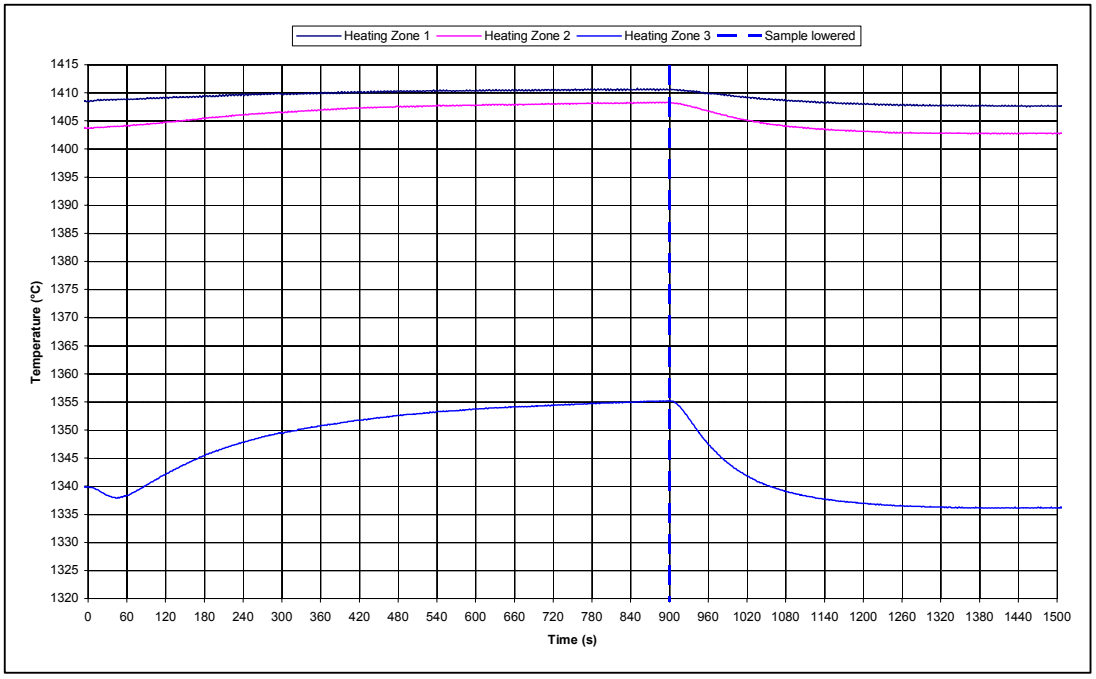

3.2. Effect of Increased Heat Transfer

Radiation heat transfer to the sample surface was calculated from the radiation network using the sample surface temperature and the furnace heating zone temperatures as inputs, at one second intervals. As a comparative example of increased heat transfer achieved with increased furnace temperature, the data for 40 mm sample layers reacted for 15 minutes at furnace heating zone 1 temperatures of 1300, 1400 and 1500°C is shown here. The sample surface temperatures, corrected for pyrometer emissivity setting and view glass transmissivity, are shown in **Fig. 25**. The incremental radiation heat transfer values calculated for each second of temperature data logged are shown in **Fig. 26**. The heating zone temperatures for these three experiments are shown in **Fig. 27 (a)-(c)**. Increased furnace temperatures result in increased radiation heat transfer to the sample surface and the heat transfer rate plot follows the sample surface temperature plot closely, indicating the strong interrelation between sample surface temperature and heat transferred. The average radiation heat transfer values over the reaction period for each sample are shown in **Table 12**. These values are equivalent to weighted average heat transfer values because the incremental radiation heat transfer values were calculated at one second intervals.

Comparison of the heap surface temperatures shown in **Fig. 25** with the heating zone temperatures shown in **Fig. 27** shows that a large temperature differential persists between the sample surface temperature and each of the heating zone temperatures.

Table 12: Average radiation heat transfer to sample surface of 40 mm layer coal-ore samples

Reaction Time (minutes)	Average kW/ m^2 at Furnace Heating Zone 1 Temperature (°C)			*ΔkW/m^2 (a)	*ΔkW/m^2 (b)
	1300°C	1400°C	1500°C		
3	-120	-181	-259	61	78
6	-127	-180	-250	53	70
9	-125	-178	-254	53	76
12	-109	-175	-211	66	36
15	-108	-169	-208	61	39

*ΔkW/m^2 (a) = (Average kW/m^2 at 1400°C furnace heating zone 1 temperature) - (Average kW/m^2 at 1300°C furnace heating zone 1 temperature)
*ΔkW/m^2 (b) = (Average kW/m^2 at 1500°C furnace heating zone 1 temperature) - (Average kW/m^2 at 1400°C furnace heating zone 1 temperature)

From **Fig. 25 and 27** the temperature differentials between the sample surface temperatures and the heating zone 1 temperatures are of the order of 200-250°C, and that between the sample surface temperatures and the heating zone 3 temperatures are 150-200°C. The temperature differentials between the heating zone 1 temperatures and the sample surface temperatures for the rest of the 40 mm layer samples are shown in **Table 13**. Also, as shown in **Fig. 24 (a)**, the initial temperature differentials in the material bed when the material layer is heated uni-directionally from the sample surface, persist when the surface temperature levels off towards a steady state value. The temperature differentials between the sample surface temperatures and the material layer bottom segment temperatures for the rest of the 40 mm layer samples are shown in **Table 13**. Hence both radiative heat transfer and conduction were limiting factors under these conditions.

Table 13: Temperature differentials for 40 mm material layers

Reaction Time (minutes)	ΔT_Top* at 1300°C	ΔT_Top* at 1400°C	ΔT_Top* at 1500°C	ΔT_Bed* at 1300°C	ΔT_Bed* at 1400°C	ΔT_Bed* at 1500°C
3	277	302	338	907	995	1053
6	259	292	312	785	888	870
9	272	303	310	677	735	700
12	229	283	262	641	639	615
15	224	266	257	537	543	421

ΔT_Top* at the furnace heating zone 1 temperature = Furnace heating zone 1 temperature – Sample surface temperature
ΔT_Bed* at the furnace heating zone 1 temperature = Sample surface temperature – Sample bottom segment temperature (30 mm from sample surface)

The difference between average radiation heat transfer values calculated for samples reacted for different periods at 1300°C and 1400°C furnace heating zone 1 temperature are similar, as shown in **Table 12**. However, for samples reacted at 1400°C and 1500°C furnace heating zone 1 temperature the difference in average radiation heat transfer values are lower at 12 and 15 minute reaction times. This is due to increased heap surface temperatures measured in the samples reacted at 1500°C furnace heating zone 1 temperature for 12 and 15 minutes, respectively. The increased surface temperatures at

12 and 15 minutes reaction time can be explained by decreased reduction rate at increased reduction extent in the top node, 70% reduction at 12 minutes reaction time and 76% reduction at 15 minutes reaction time, resulting in decreased energy utilisation for reduction and consequently increased energy utilisation for heating the material bed.

Fig. 25: Sample Surface Temperatures at different furnace heating zone temperatures for 40 mm coal-ore samples reacted for 15 minutes

(Corrected for pyrometer emissivity setting and view glass transmissivity)

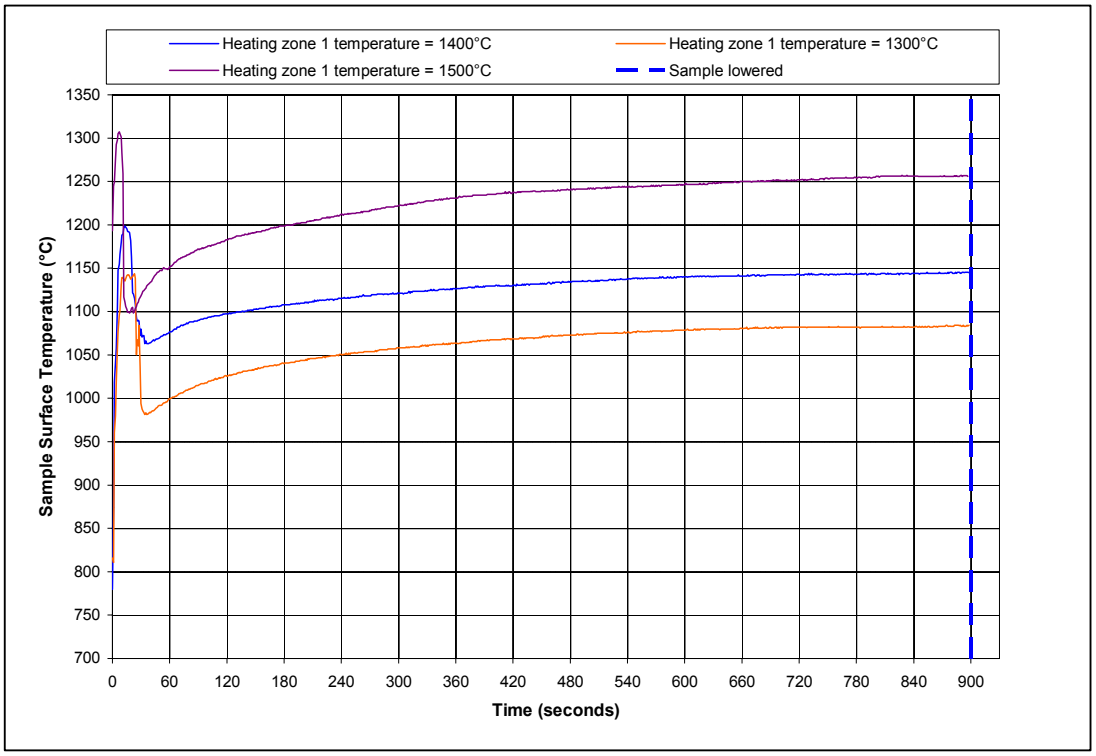

Fig. 26: Radiation heat transfer to sample surface at different furnace heating zone 1 temperatures for 40 mm coal-ore samples reacted for 15 minutes

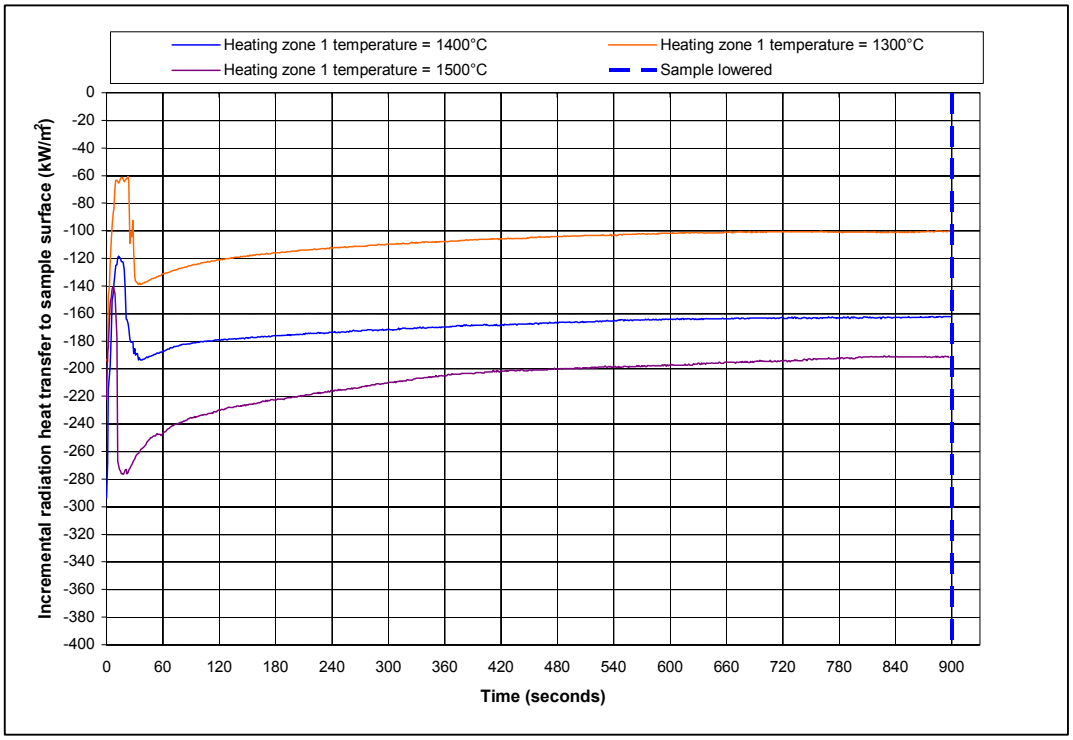

Fig. 27: Heating zone temperatures at different furnace heating zone 1 temperatures for 40 mm coal-ore samples reacted for 15 minutes

(a) Heating zone 1 temperatures

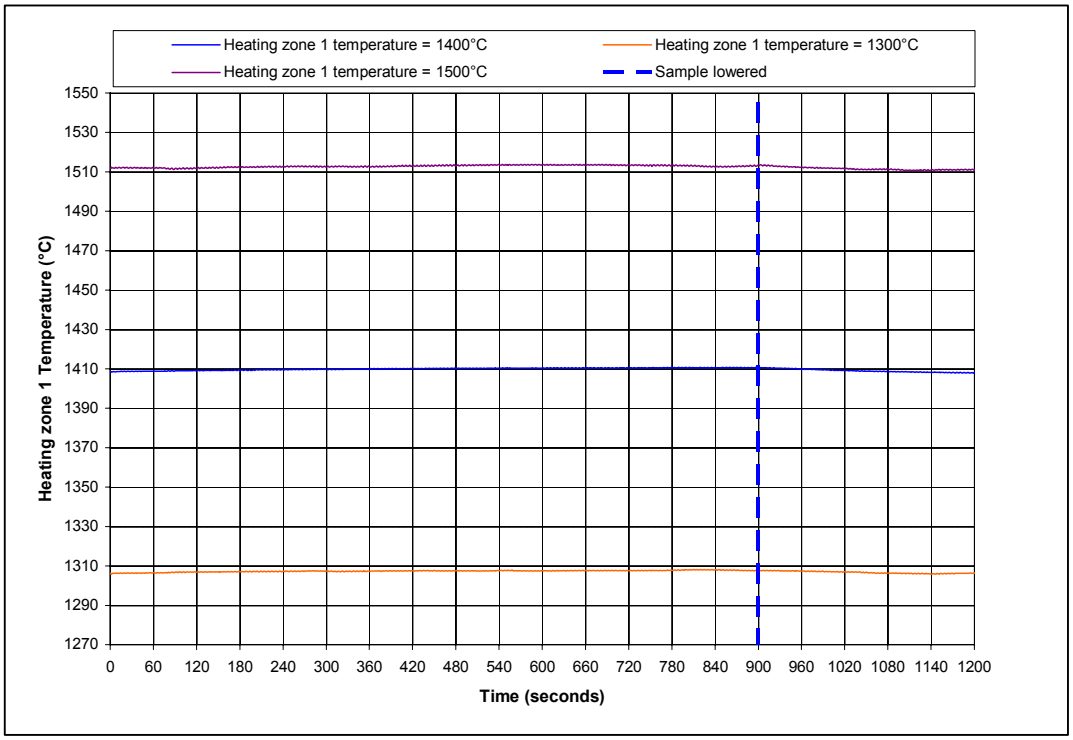

(b) Heating zone 2 temperatures

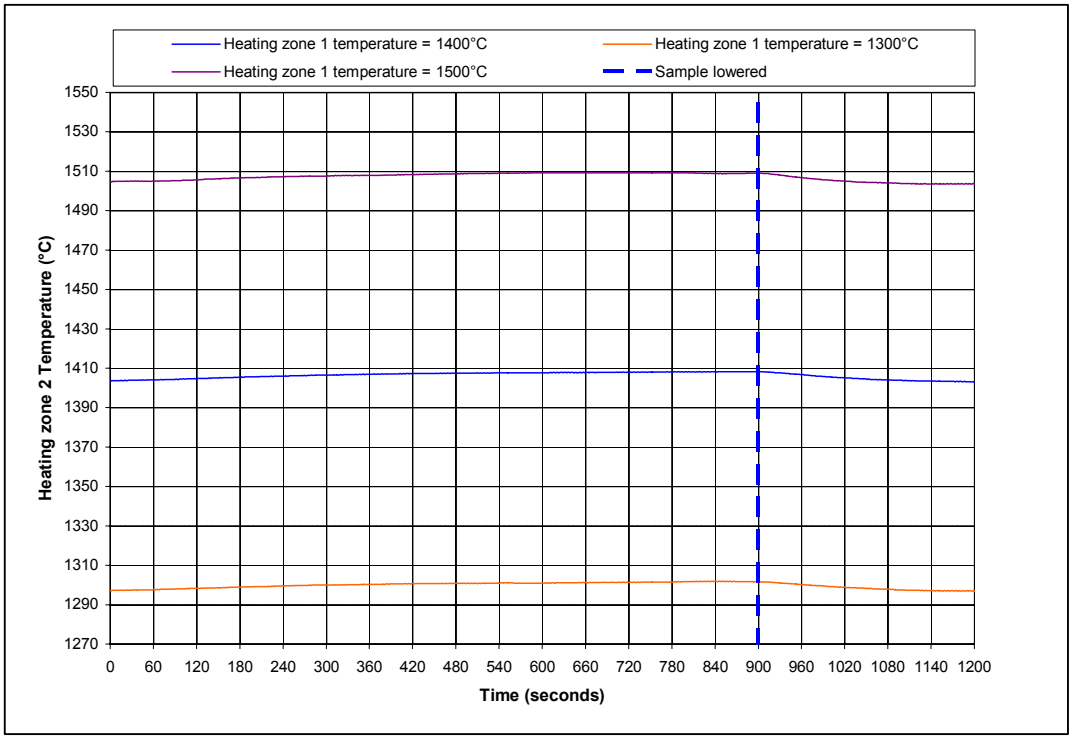

(c) Heating zone 3 temperatures

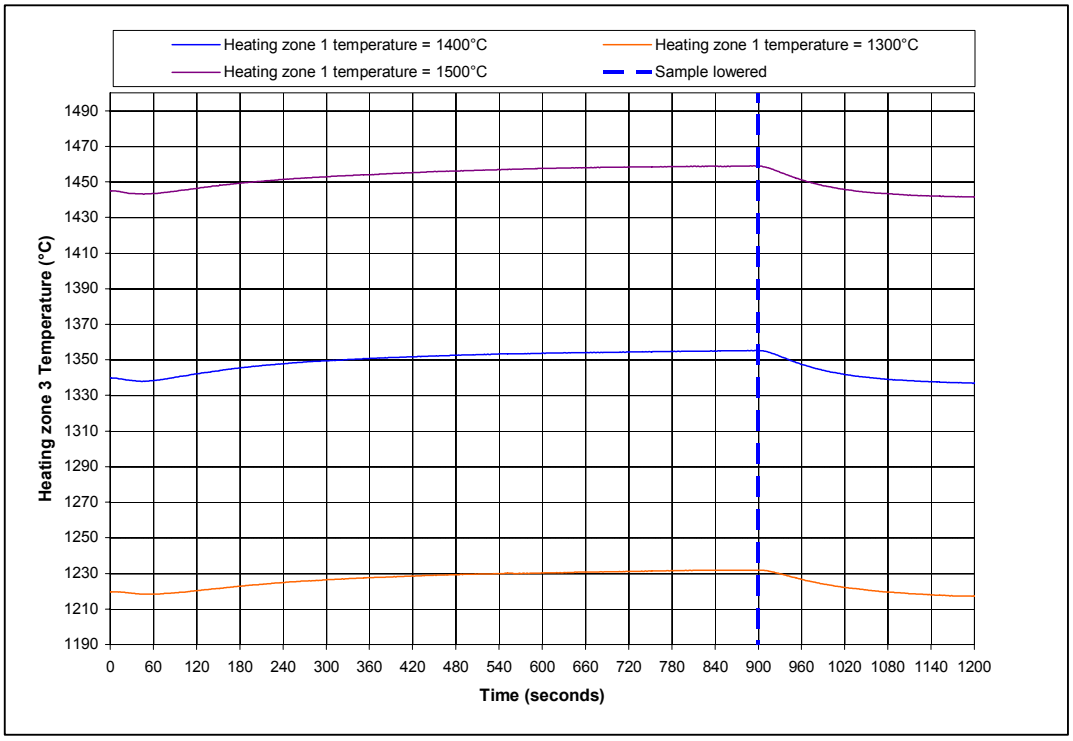

Fig. 28 (a) and (b) show the reduction extent and carbon consumption for the whole sample. Carbon consumption and reduction extent per sample segment, in **Fig. 29** and **Fig. 30,** indicate that very little reduction takes place in the middle and bottom segments of the sample. The reduction extent for each sample segment was calculated from the forms of iron analyses of the reacted material of the particular segment. Because little reduction took place in the middle and bottom segments the carbon consumption values in these segments are erratic, compared to that in the top segment. For ten of the segment analyses the carbon consumption values for the middle and bottom segments are negative by 0.03 to 0.27 g carbon, compared with 1.6 and 1.8 g C input to the middle and bottom segments.

Fig. 28 (a): Composite reduction extent

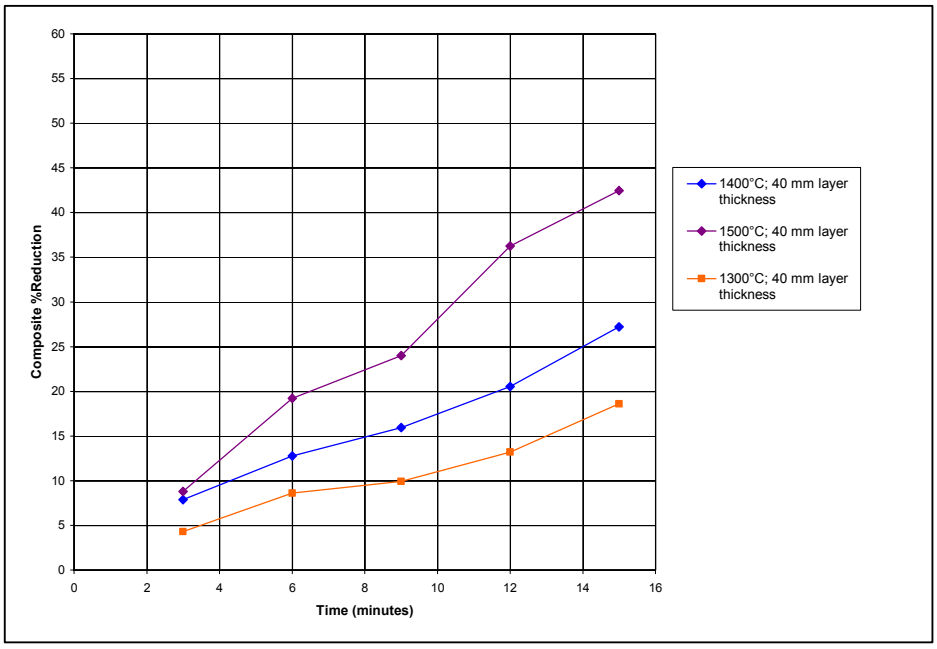

Fig. 28 (b): Composite carbon consumption

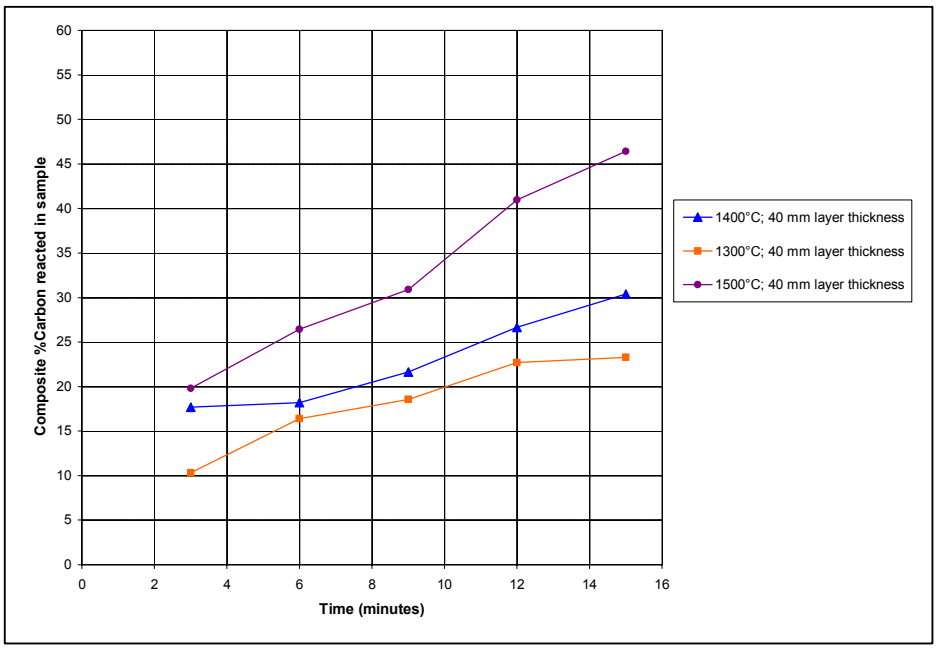

Fig. 29: Reduction extent for each material layer segment

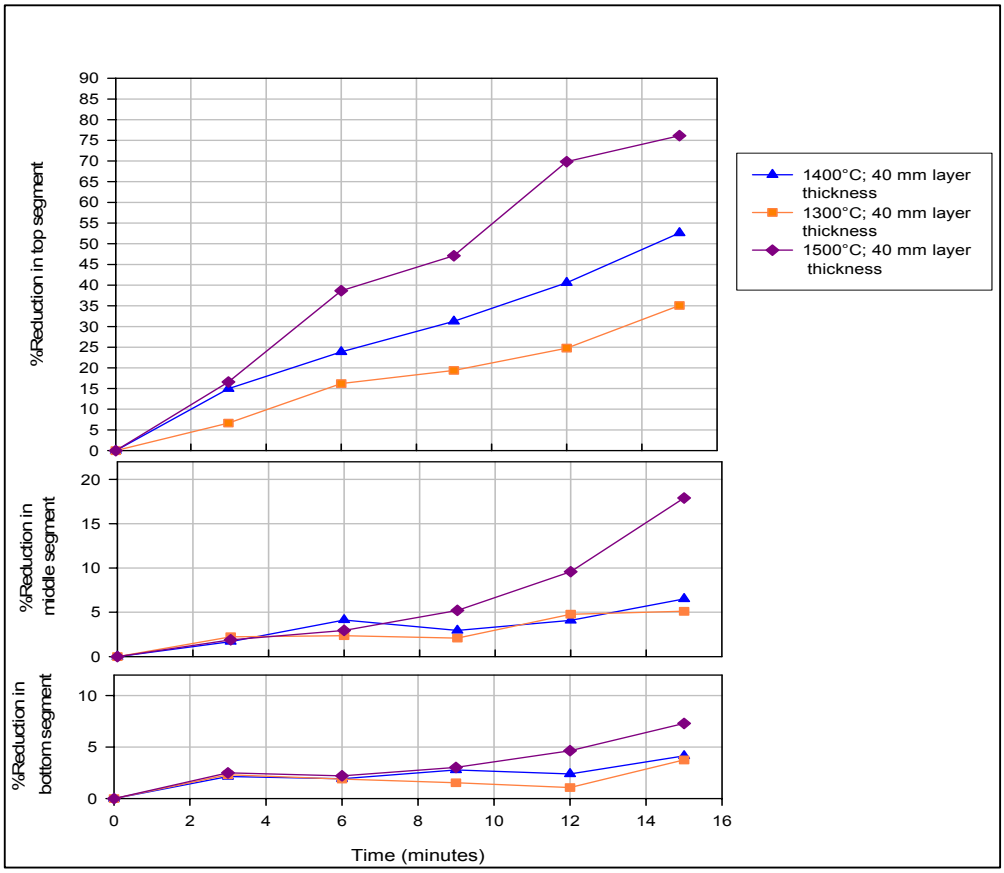

Fig. 30: Carbon consumption for each material layer segment

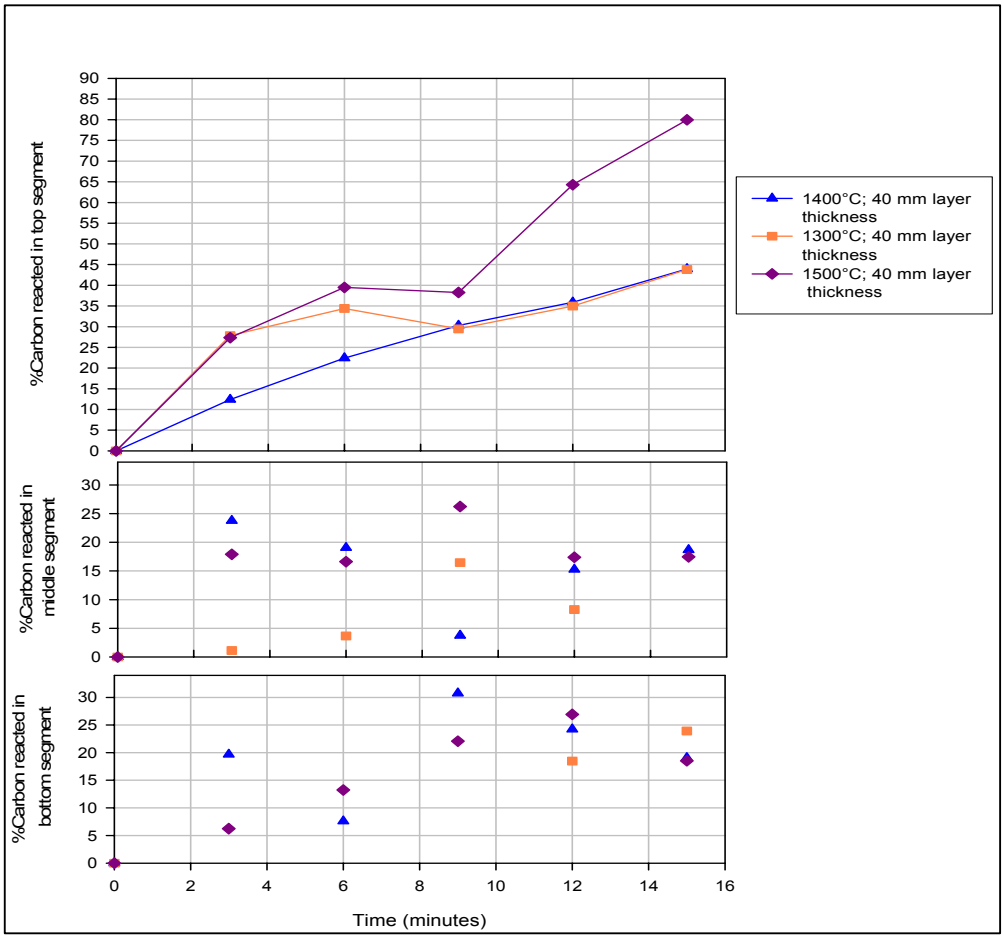

The temperature in each material layer segment at the end of the reaction period is shown in **Fig. 31**. At three minutes reaction time the material segment temperatures are similar, and up to nine minutes reaction time the material segment temperatures at 1300°C and 1400°C heating zone one temperatures are similar. Beyond three minutes reaction time material segment temperatures at 1500°C heating zone one temperature are distinctly higher compared to the rest of the segment temperatures, for the same reaction time.

Fig. 31: Temperature for each material layer segment at the end of the reaction time

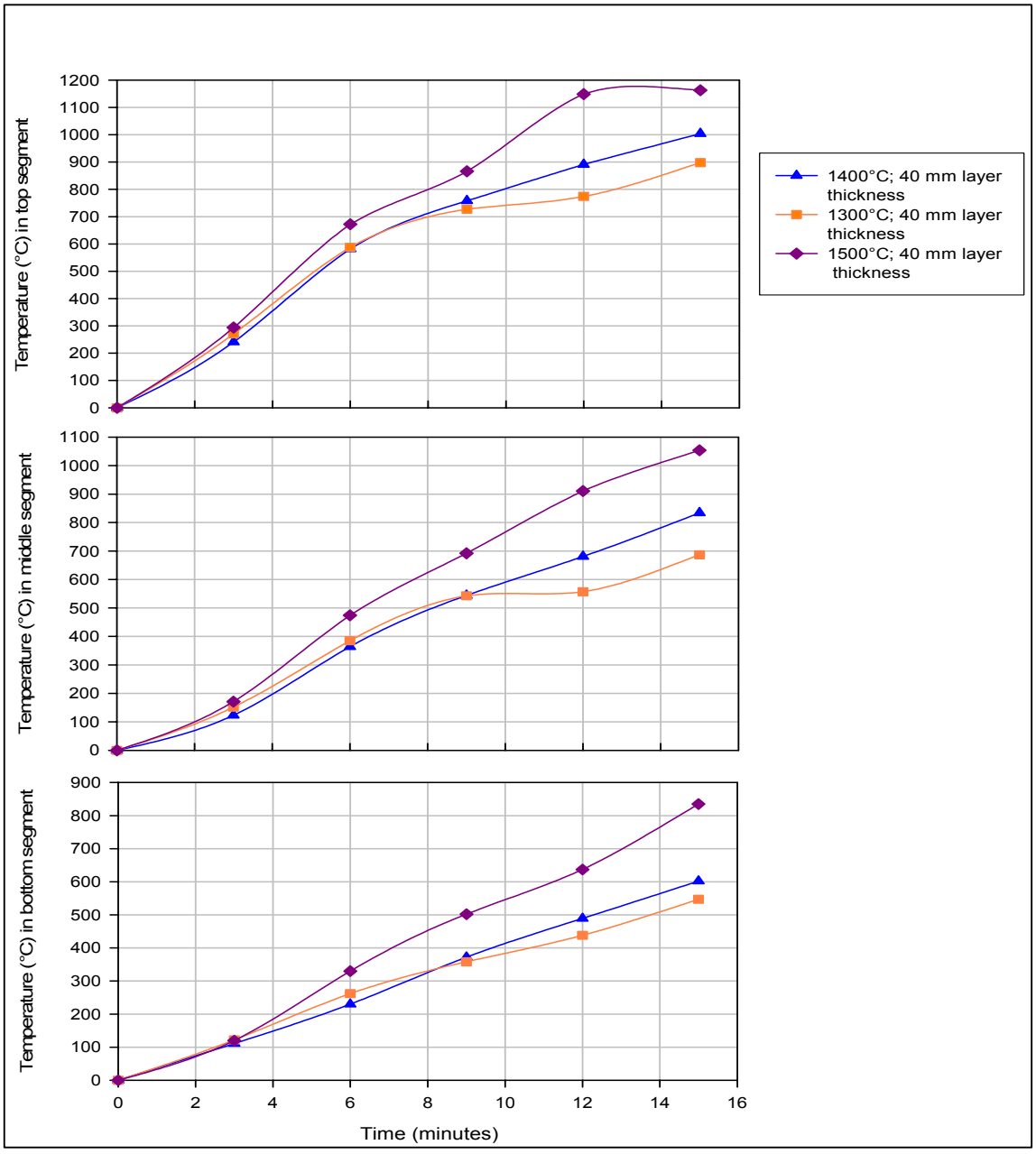

In addition to the presence of large persistent temperature differentials between the sample surface and the heating zones, as well as temperature differentials within the material layer, another indicator of heat transfer control is increased reaction rate attained at increased heat transfer rate. This is shown in **Fig. 32** below.

Fig. 32: Total radiation heat transferred vs. Composite %Reduction

(Number inside square frame shows reaction time in minutes)

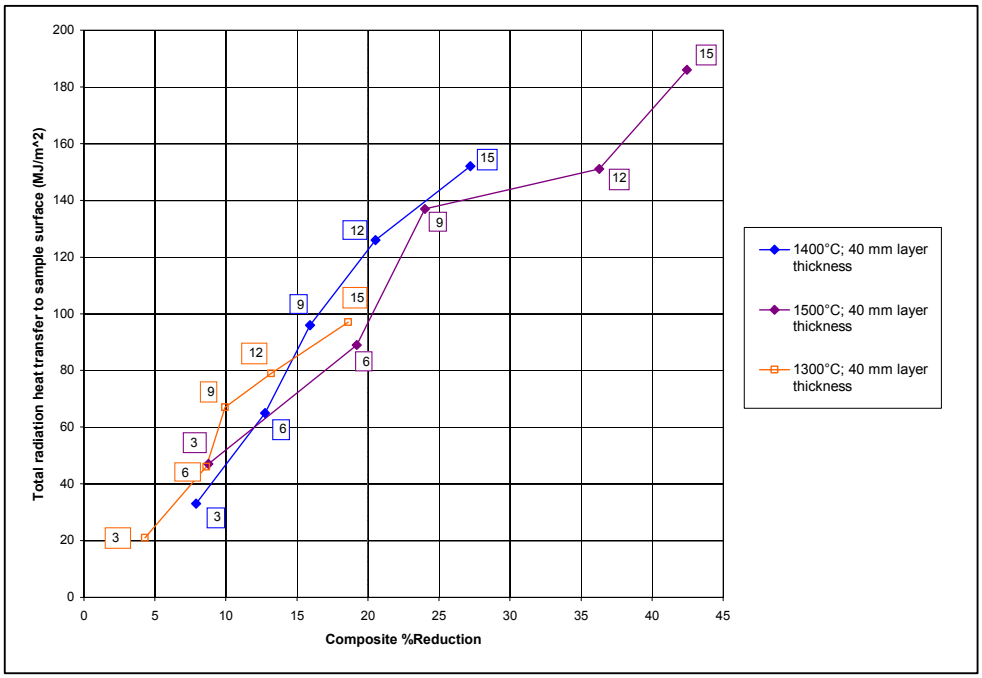

3.3. Effect of Layer Thickness

At 1400°C heating zone 1 temperature material layer thickness samples of both 40 mm and 16 mm were reacted. Increased reaction extent in 16 mm material layers, as compared to that in 40 mm material layers, for the same heat input conditions shows conduction heat transfer control. The sample temperature profiles for 15 minutes reaction time of a 40 mm and 16 mm material layer, respectively, are shown in **Fig. 33 (a) and (b).** The associated heating zone temperatures are compared in **Fig. 34 (a) and (b)**. The steady state surface temperature for the 16 mm layer material is 26°C higher than that of the 40 mm layer material. The bed temperatures in the 16 mm layer at 4 mm and 10 mm from the sample surface are higher than those in the 40 mm layer.

The product gas profiles for 40 mm material layers and 16 mm material layers were similar. The difference is that product gas of higher reducing potential was produced in the 16 mm layers, as compared to that from the 40 mm layers. This is shown in **Fig. 35 (a) and (b)** where the $\%CO/(\%CO+\%CO_2)$ ratio in the product gas, for each experiment, is compared to the equilibrium ratio for reduction of FeO by CO, reaction (20), and the equilibrium ratio for gasification, reaction (21). The equilibrium $\%CO/(\%CO+\%CO_2)$ values were calculated at the material bed temperatures measured over the 15 minute reaction time. The calculations were done for the longest reaction time of 15 minutes only because the temperature profiles for reaction times smaller than 15 minutes are represented by the 15 minute reaction time temperature profiles as well. The heat capacity values,

standard enthalpy and entropy values used to calculate the enthalpy and entropy of reactions (20) and (21) are shown in **Appendix XII**. A linear fit of the free energy values was made for each reaction as shown in **Appendix XII**.

$$FeO_{(s)} + CO_{(g)} = Fe_{(s)} + CO_{2(g)} \quad (20)$$

$$CO_{2(g)} + C_{(s)} = 2CO_{(g)} \quad (21)$$

At the sample surface temperature the product gas %CO/(%CO+%CO_2) ratio for the 16 mm and 40 mm layers experiments plot in-between the equilibrium ratios of reactions (20) and (21). If the reduction reaction, reaction (20), was slowest the product gas CO content would be at the gasification reaction equilibrium which is 100%CO at the sample surface temperatures. If the gasification reaction was slowest the product gas CO content would be at the equilibrium %CO/(%CO+%CO_2) ratio of the reduction reaction, reaction (20). The product gas composition does not follow either equilibrium %CO/(%CO+%CO_2) ratio exclusively, indicating the interdependence of reactions (20) and (21) at the sample surface.

Fig. 36 shows the comparative reduction extent. The reduction extent for the 16 mm layer is 8% higher than that of the top layer for the 40 mm layer material sample for reaction times 9, 12 and 15 minutes. At reaction times below 6 minutes the reduction extent is similar. **Fig. 37 (a) and (b)** shows the %Carbon and mass carbon reacted in the top node in the 40 mm material layer, compared to that in the 16 mm layer. The top node comprises 46% of the 40 mm sample height, that is 18 mm. It is seen that the rate of carbon consumption is similar, but the carbon consumption is higher in the 16 mm material layer in accordance with the increased reduction extent achieved in the 16 mm layer. Heat transfer rates to the 16 mm material layer were lower compared to the 40 mm layer material, due to the slightly higher sample surface temperature and 10°C lower heating zone 3 temperatures. **Fig. 38** shows the average heat transferred to the sample for a 40 mm layer as compared to that for a 16 mm layer.

Fig. 33 (a): Temperatures of 40 mm layer thickness of coal-ore mixture reacted at 1400°C for 15 minutes.

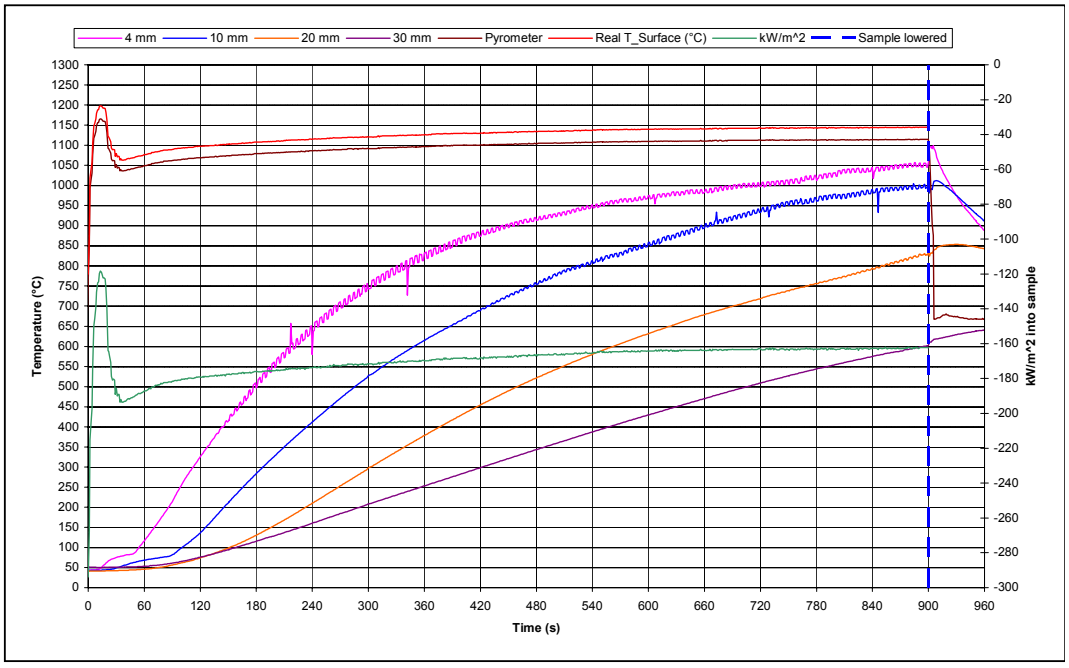

Fig. 33 (b): Temperatures of 16 mm layer thickness of coal-ore mixture reacted at 1400°C for 15 minutes.

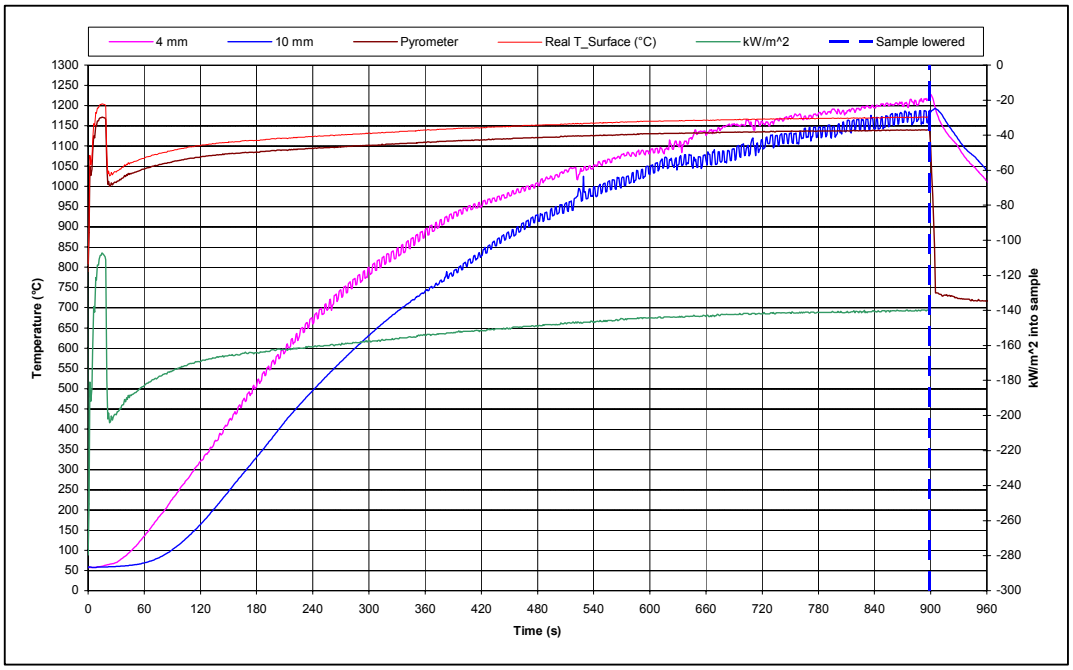

Fig. 34 (a): Comparison of furnace tube temperatures for 40 mm vs. 16 mm

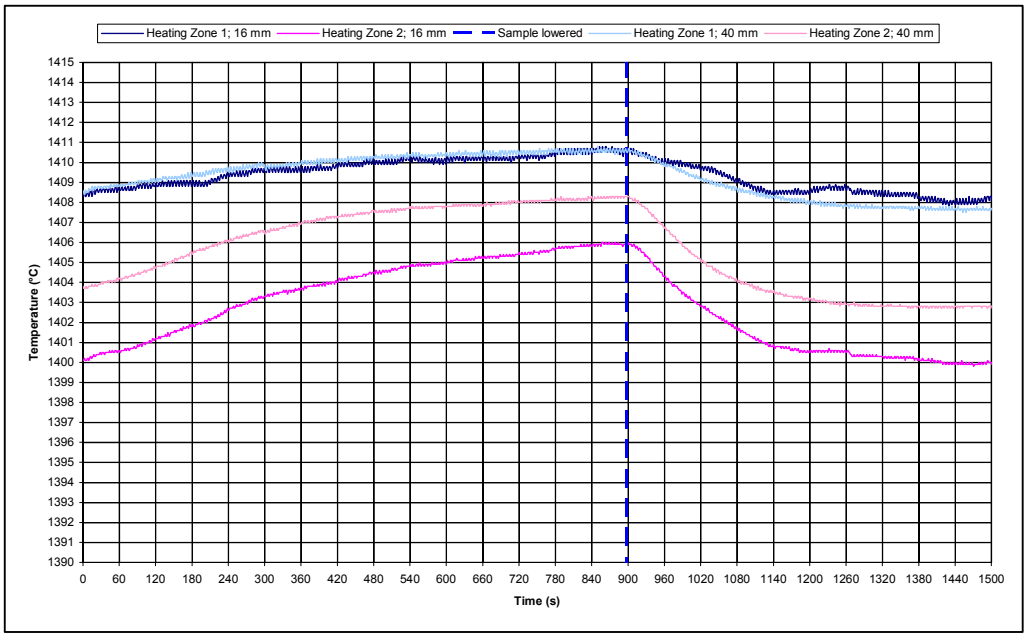

Fig. 34 (b): Comparison of furnace tube temperatures for 40 mm vs. 16 mm (Heating zone 3)

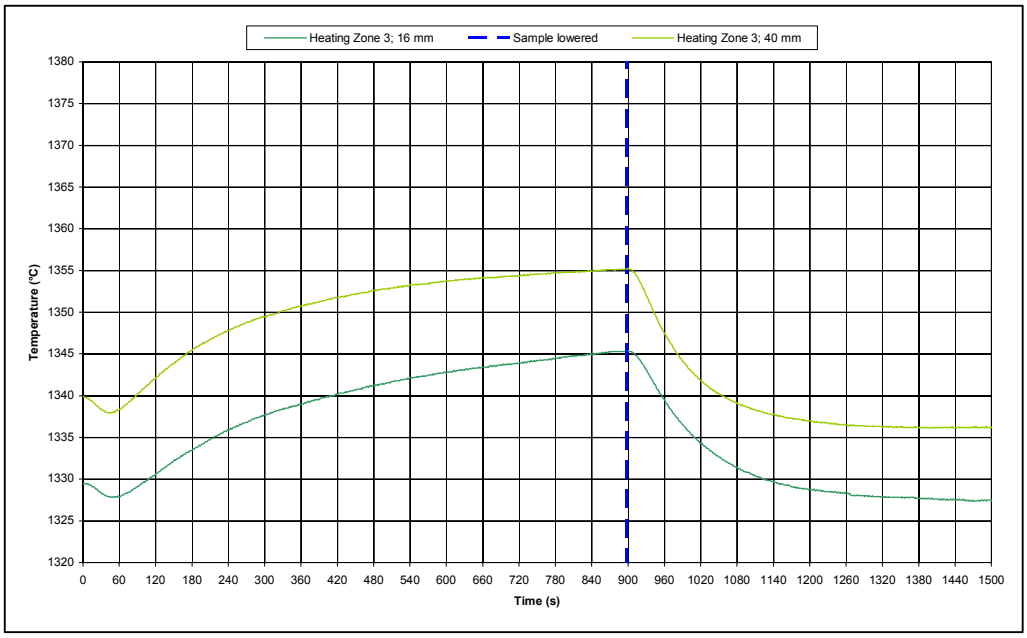

Fig. 35 (a): %CO/(%CO+CO_2) in product gas: 15 minute reaction time at 1400°C furnace temperature for 40 mm material layer

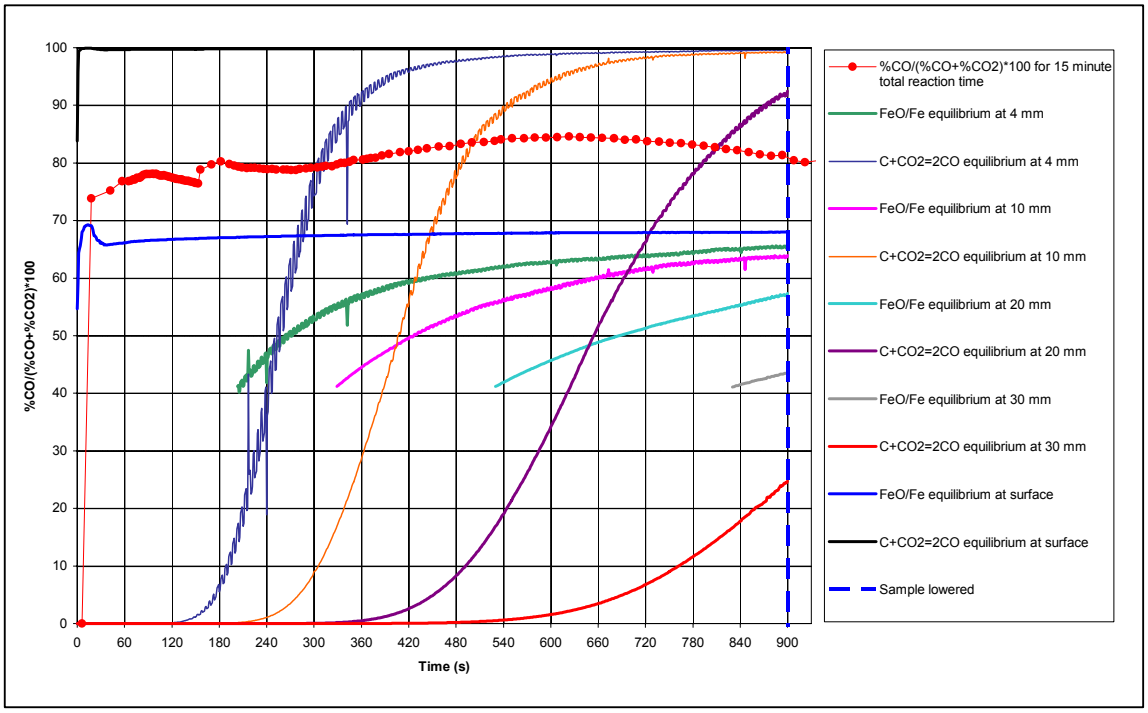

Fig. 35 (b): %CO/(%CO+CO_2) in product gas: 15 minute reaction time at 1400°C furnace temperature for 16 mm material layer

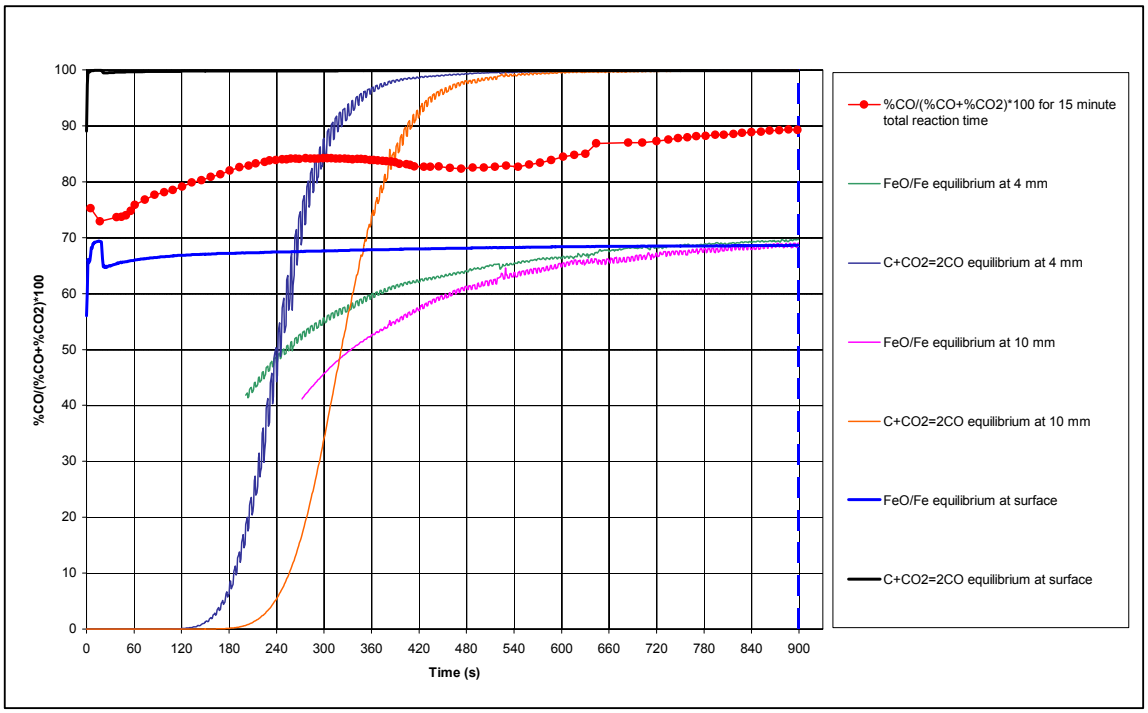

Fig. 36: Comparison %Reduction in top segment of 40 mm material layer vs. 16 mm material layer *(Top segment of 40 mm material layer is 18 mm)*

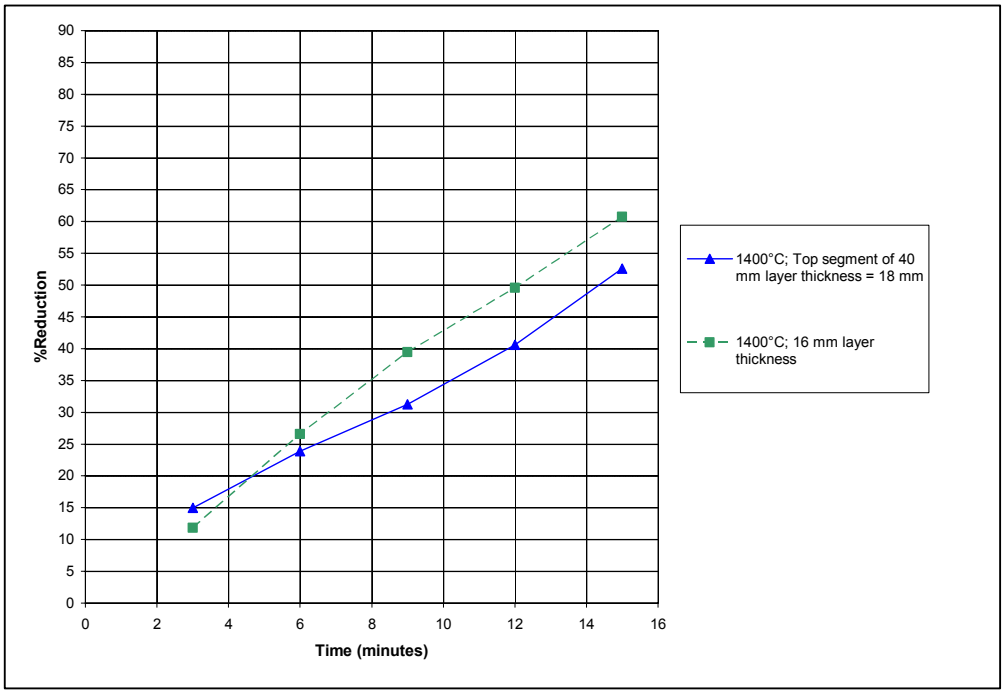

Fig. 37 (a): Comparison %Carbon for top segment of 40 mm to 16 mm material layer thickness

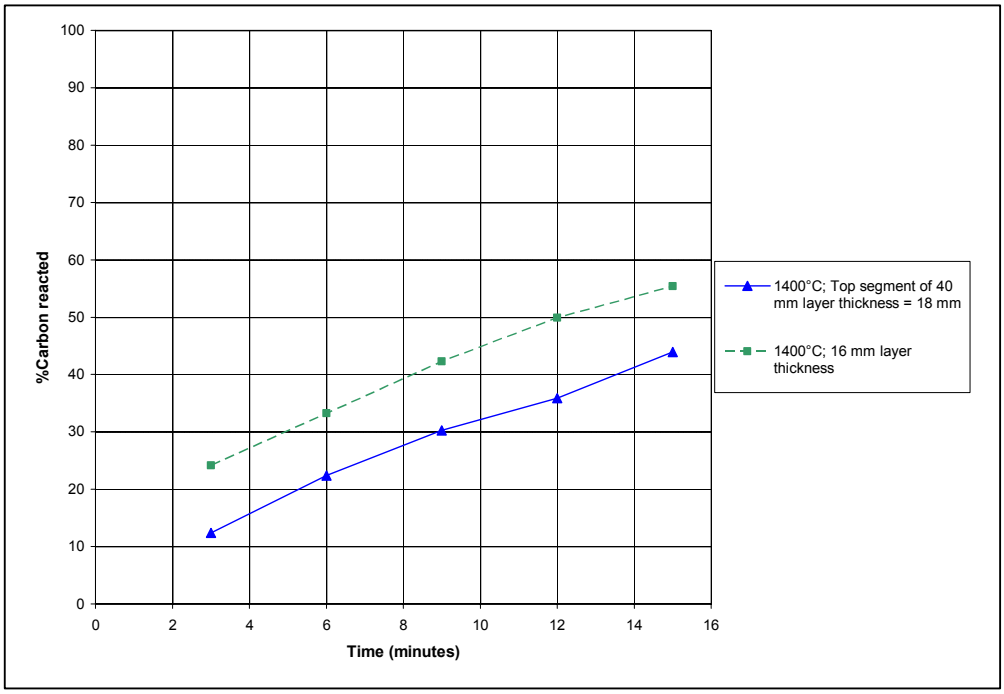

Fig. 37 (b): Comparison mass carbon for top segment of 40 mm to 16 mm material layer thickness

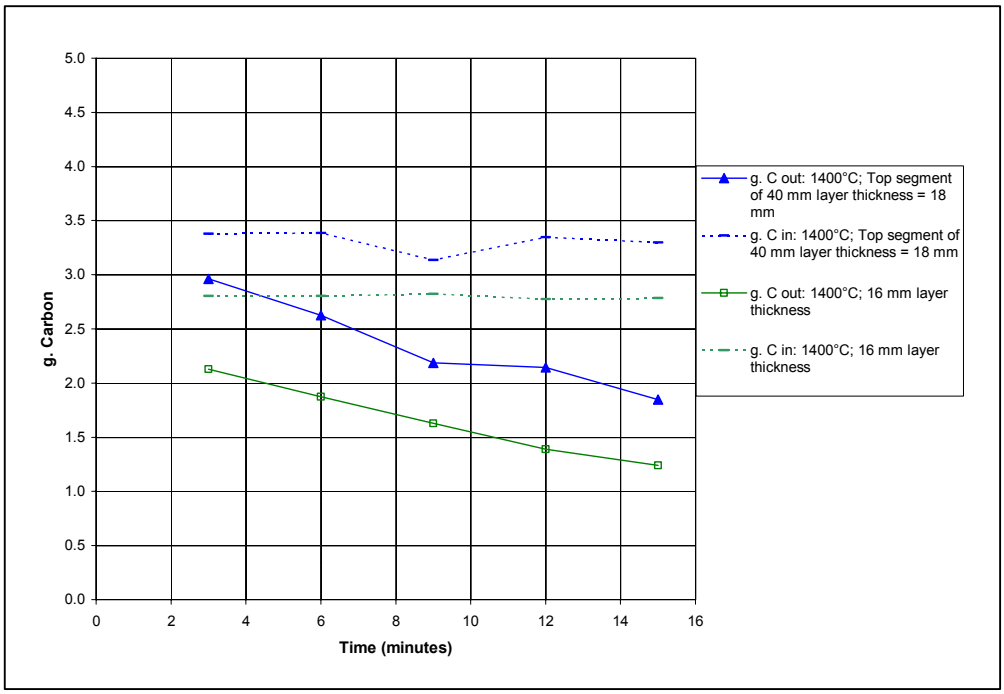

Fig. 38: Average radiation heat transfer to sample surface: Top segment of 40 mm material layer vs. 16 mm material layer

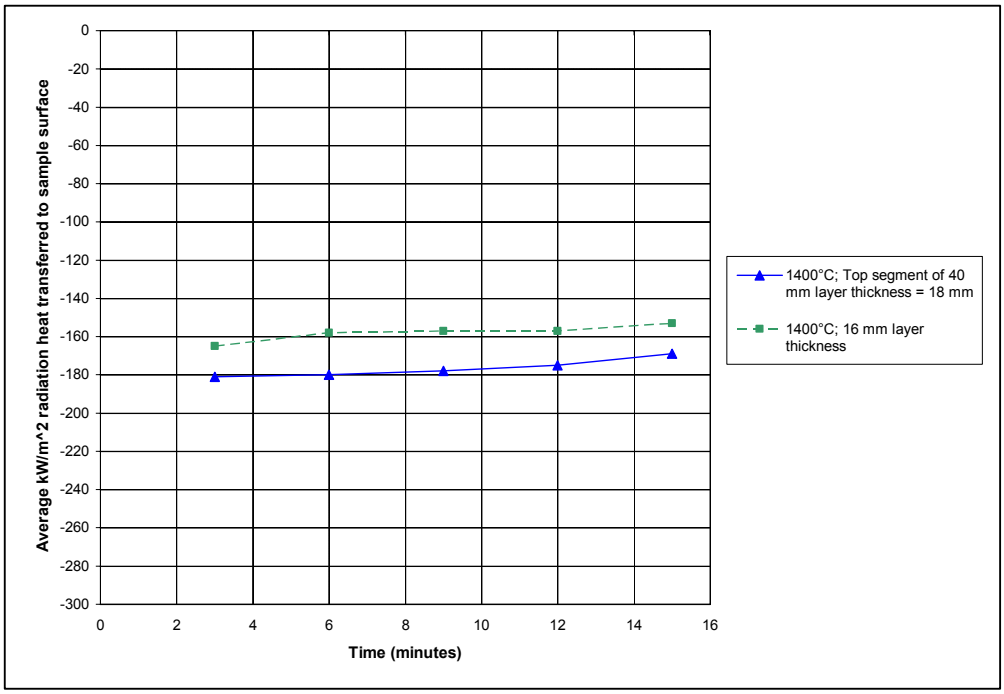

3.4. Effect of Volatiles in Coal

The composition and flow rate of the gas product released from the heap surface are important input information for the process energy balance. The contribution of coal devolatilisation to the product gas was isolated by heating coal-alumina samples instead of coal-ore samples. This approach has been used by Dey *et al.* (1993), Wang *et al.* (1997, 1998), Dutta and Gosh (1994), Sohn and Fruehan (2006a). The coal-alumina samples were heated until negligible volatile content was observed in the product gas analyses. The volatile components in the product gas for coal reacted at different furnace temperatures are shown in **Fig. 44-46**, with the associated material bed temperatures. Although the product gas analyses show that the coal volatiles consisted largely of hydrogen on volume basis, the hydrogen portion decreases from 26 mass% at 1300°C furnace temperature to 12 mass% and 13 mass% at 1400°C and 1500°C furnace temperature as the mass of CO and CO_2 increased with increasing furnace temperature. Negligible methane was measured in the product gas. This does not mean that methane is not one of the devolatilisation products as carbon deposition onto the crucible walls was observed whenever coal was reacted. An example of carbon deposition is shown in **Fig. 39**, compared to samples of char-ore mixtures reacted under the same conditions, shown in **Fig. 40**.

The molar quantities of product gas for the total reaction time, at each heating zone temperature, are shown in **Fig. 41**, indicating increased H_2, H_2O and CO release with increased reaction temperature. The endpoint reaction temperatures in the coal-alumina material layer, shown in **Fig. 44-46**, is in excess of 900°C, indicating that devolatilisation should be complete in the samples. The total mass of carbon reporting to the product gas is shown in **Fig. 42**, as calculated from the product gas analyses and the carbon analyses of the devolatilised sample. The mass carbon to gas for devolatilisation, shown in **Fig. 42**, corresponds well for 1500°C, and not well for 1300°C and 1400°C. The calculations of mass loss to the gas, as shown in **Fig. 43**, correspond better for reaction at 1300°C and 1400°C, but not for 1500°C. Coal volatile content values calculated from the mass loss measured are 24%, 31% and 28% at 1300°C, 1400°C and 1500°C vs. 14%, 32% and 64% calculated from the product gas analyses. The increased volatile gas release with increased reaction temperature and increased heating rates has been reported in literature (Desypris *et al*., 1982).

Fig. 39: Carbon deposition on crucible walls for coal-ore samples

Fig. 40: No carbon deposition on crucible walls for char-ore samples

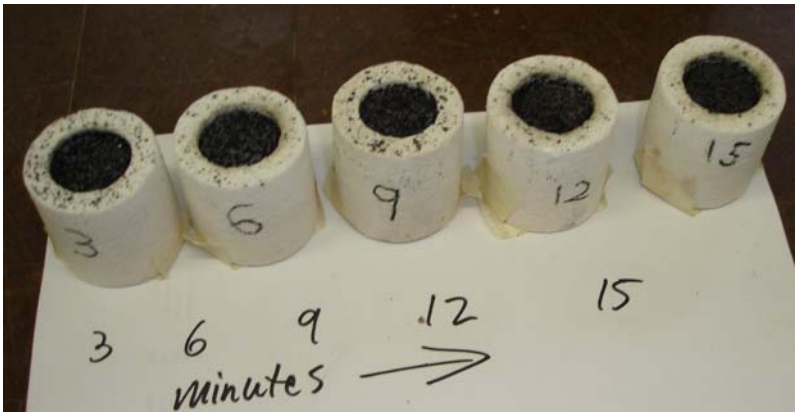

Fig. 41: mol to gas in coal devolatilisation

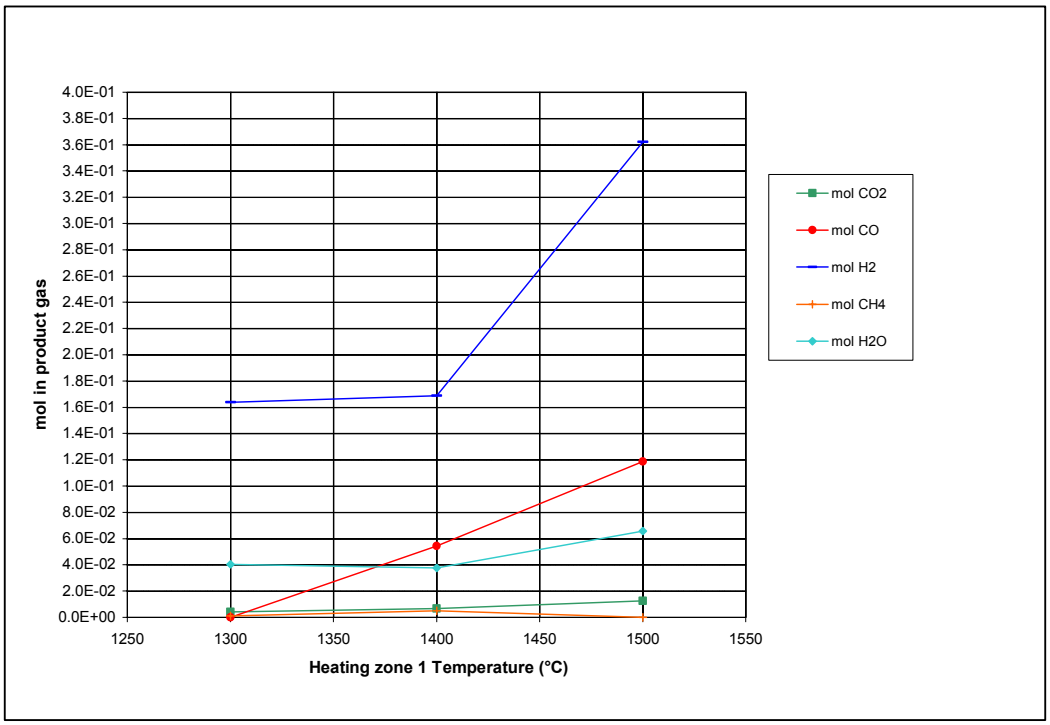

Fig. 42: Mass carbon to product gas in coal devolatilisation

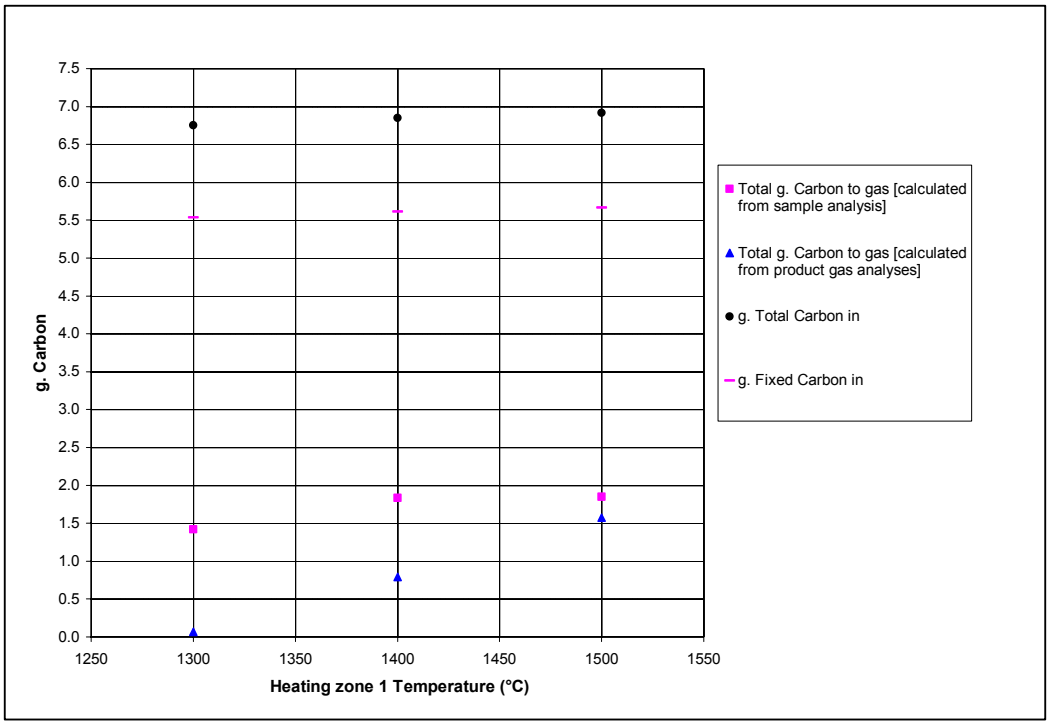

Fig. 43: Mass% of initial mass coal to product gas in coal devolatilisation

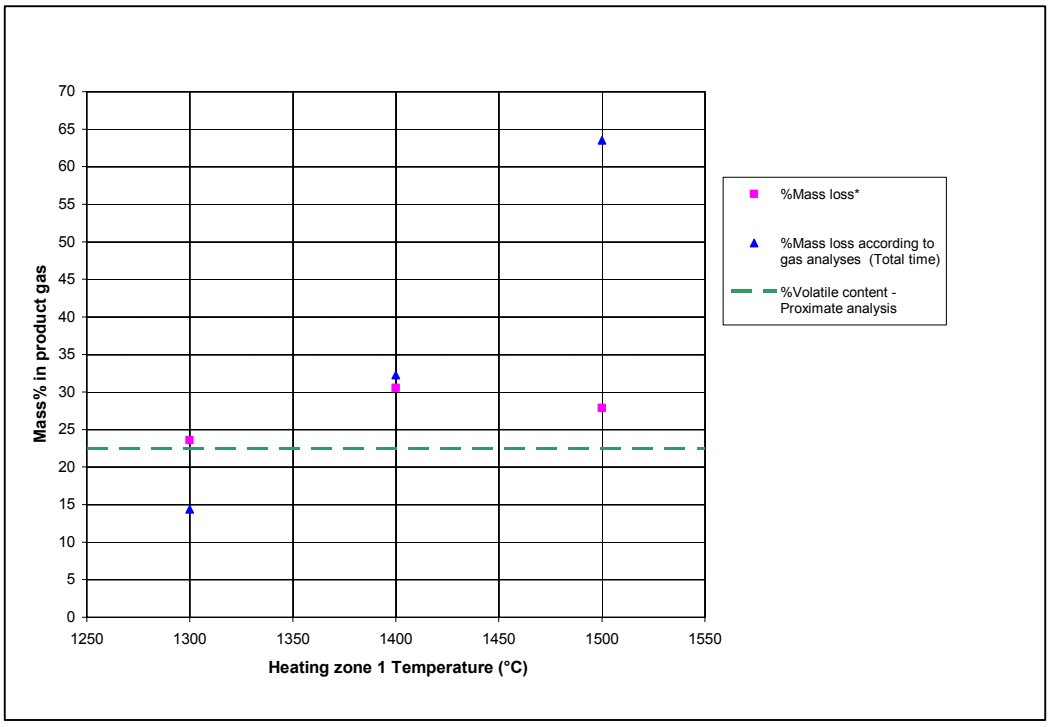

*Mass loss = (mass in) – (mass out); (mass in) calculated from alumina mass balance; (mass out) calculated from sample mass measured after sample split and then corrected for fibreboard carry over.

The following reactions are possible reactions of devolatilisation in the absence of oxygen. The temperatures at which the forward reaction can take place according to thermodynamics are indicated below; the thermodynamic calculation data is shown in **Appendix XII**.

$$CH_4(g) + H_2O(g) = CO(g) + 3H_2(g) \; ; \text{T} > 617°\text{C} \quad (22)$$

$$CH_4(g) = C(s) + 2H_2(g) ; \text{T} > 542°\text{C} \quad (23)$$

$$CH_4(g) + CO_2(g) = 2CO(g) + 2H_2(g) ; \text{T} > 643°\text{C} \quad (24)$$

$$H_2O(g) + CO(g) = CO_2(g) + H_2(g) ; \text{T} < 848°\text{C} \quad (25)$$

$$H_2O(g) + C(s) = CO(g) + H_2(g) ; \text{T} > 674°\text{C} \quad (26)$$

$$CO_2(g) + C(s) = 2CO(g) ; \text{T} > 706°\text{C} \quad (27)$$

(s) = solid material

(g) = gas phase material

The picture in **Fig. 39** shows that the carbon deposition profile along the height of the crucible extended further down the crucible with increased reaction time. This indicates that carbon deposition is associated with increased temperature via reaction (23) and (26) not via reaction (27). Further indication that carbon deposition is not due to reaction (27), as the sample was cooled, is that the picture in **Fig. 40** for ore-char samples shows no deposited carbon.

For devolatilisation at 1300°C heating zone 1 temperature, as shown in **Fig. 44**, the absence of CO and/or CH_4 in the product gas indicates that the only reactions that proceeded significantly are H_2 formation from reaction (23) forward and/or direct H_2 release from coal. The small quantities of CO_2 formed indicate that reaction (25) did not proceed to a significant extent. Devolatilisation at 1400°C and 1500°C is more complex because CO is present in the product gas. As is the case for devolatilisation at 1300°C, no significant quantity of CH_4 is present in the product gas.

The CO can be the product of reactions (22), (24), (26) and (27) at temperatures below 848°C. **Fig. 45** and **Fig. 46** show the H_2/CO ratio in the product gas, and the time at which changes in the H_2/CO ratio took place are indicated by vertical broken lines. The corresponding time markings are indicated on the material temperature graphs, adjusted for the residence time of gas in the furnace set-up. For reaction at 1400°C this ratio is initially higher than four, and then levels off to a value of three until a dip in the ratio at 799 seconds, indicated by the vertical broken green line in the product gas composition graph. The ratio of three indicates that reaction (22) is the dominant reaction. At 927 seconds, indicated by the vertical broken pink line, the H_2/CO ratio recovers to 3 and continues to increase beyond this value to the end of the devolatilisation.

For devolatilisation at 1500°C furnace temperature the H_2/CO ratio is close to three from the beginning of reaction. Three changes in the H_2/CO ratio are indicted by the time markings on the gas composition and bed temperature graphs. The first change is a slight increase in the H_2/CO ratio at 720 seconds on the product gas composition graph, indicated by the vertical broken red line, and can be explained by the bottom segment temperature reaching 551°C to release H_2 from the decomposition of CH_4, reaction (23). Then the H_2/CO ratio increases to four, and suddenly drops back to three at 912 seconds, indicated by the vertical broken green line. At 1011 seconds the H_2/CO ratio increases as the product gas CO content decrease more quickly than the H_2 product gas content. The latter effect can only be explained from reaction (23) because this is the only reaction to form H_2 alone.

From the above the conclusion is that significant H_2 is released in coal devolatilisation over 3-15 minute reaction periods of coal containing material layers of 40 mm reacted at 1300, 1400 and 1500°C furnace temperatures. The release of H_2 is due to decomposition of CH_4 and/or direct release of H_2 from the coal.

Fig. 44 (a): Coal devolatilisation in coal-alumina sample reacted at 1300°C: Temperatures

(Horisontal temperature lines for reactions (22) to (27) indicates the equilibrium temperatures)

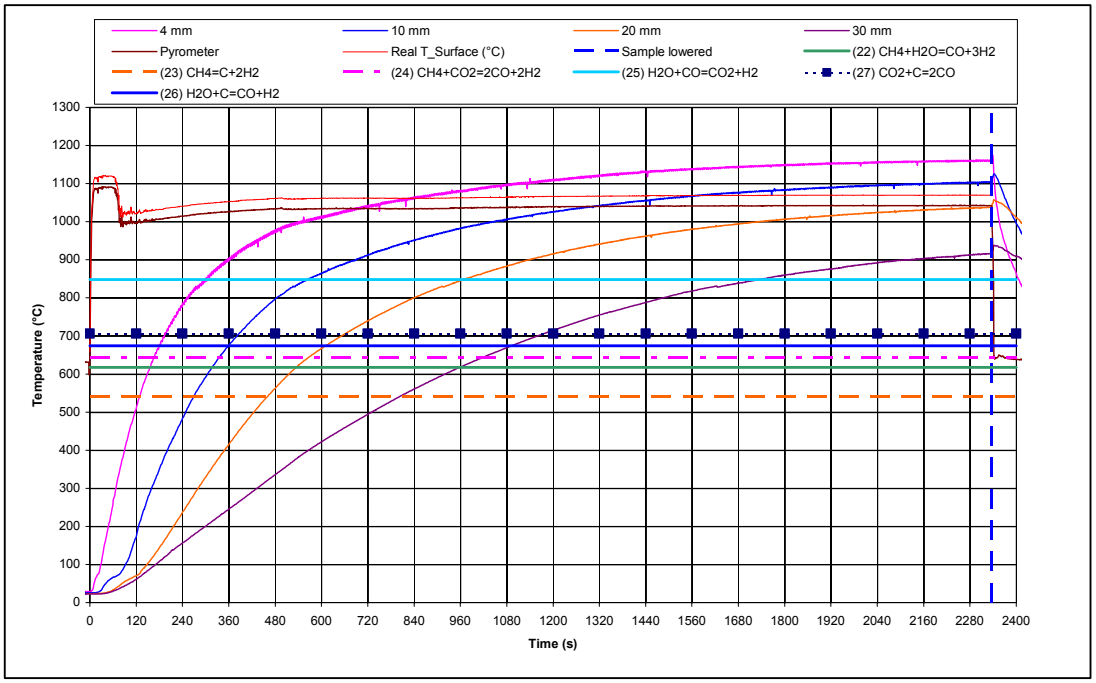

Fig. 44 (b): Coal devolatilisation in coal-alumina sample reacted at 1300°C: Product gas

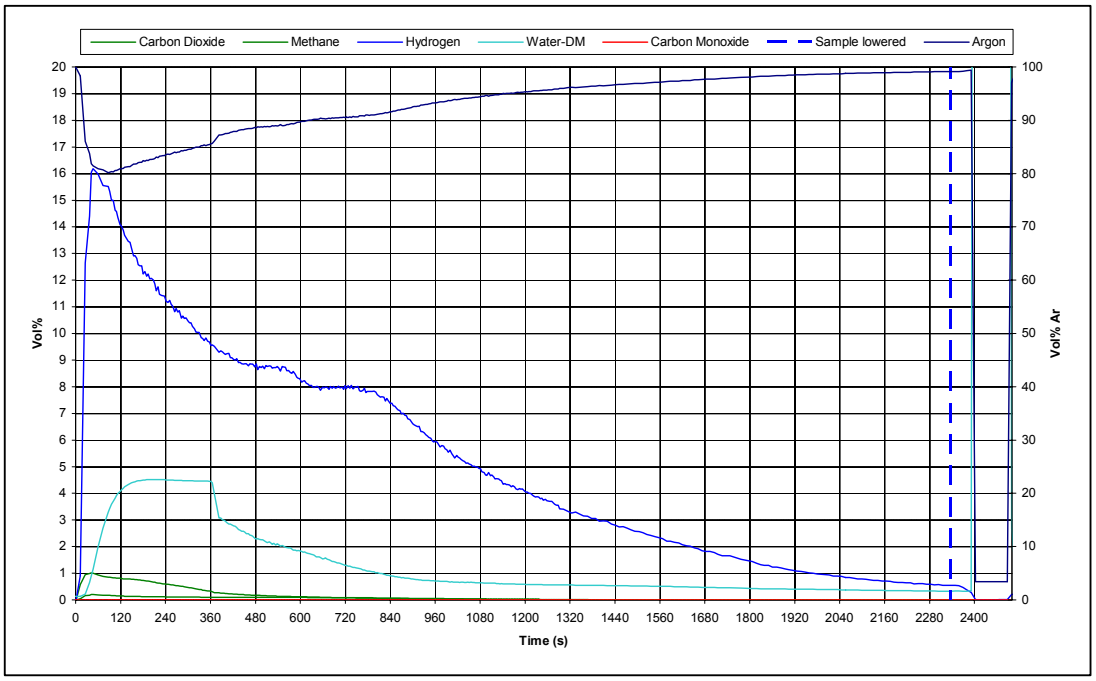

Fig. 45 (a): Coal devolatilisation in coal-alumina sample reacted at 1400°C: Temperatures

(Horisontal temperature lines for reactions (22) to (27) indicates the equilibrium temperatures)

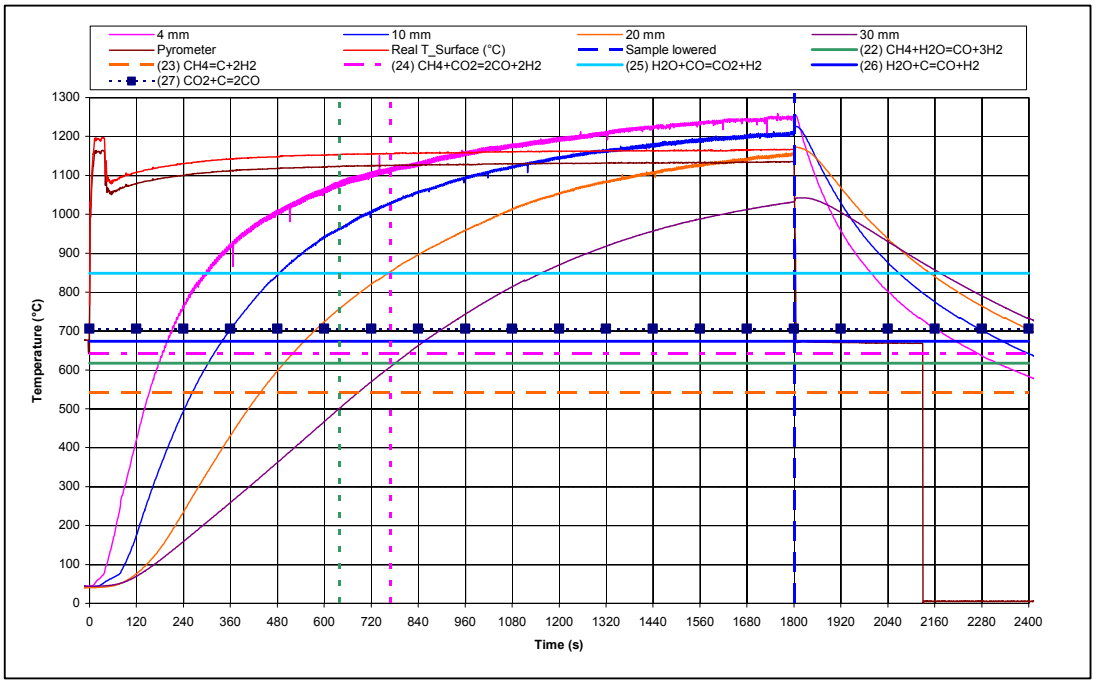

Fig. 45 (b): Coal devolatilisation in coal-alumina sample reacted at 1400°C: Product gas

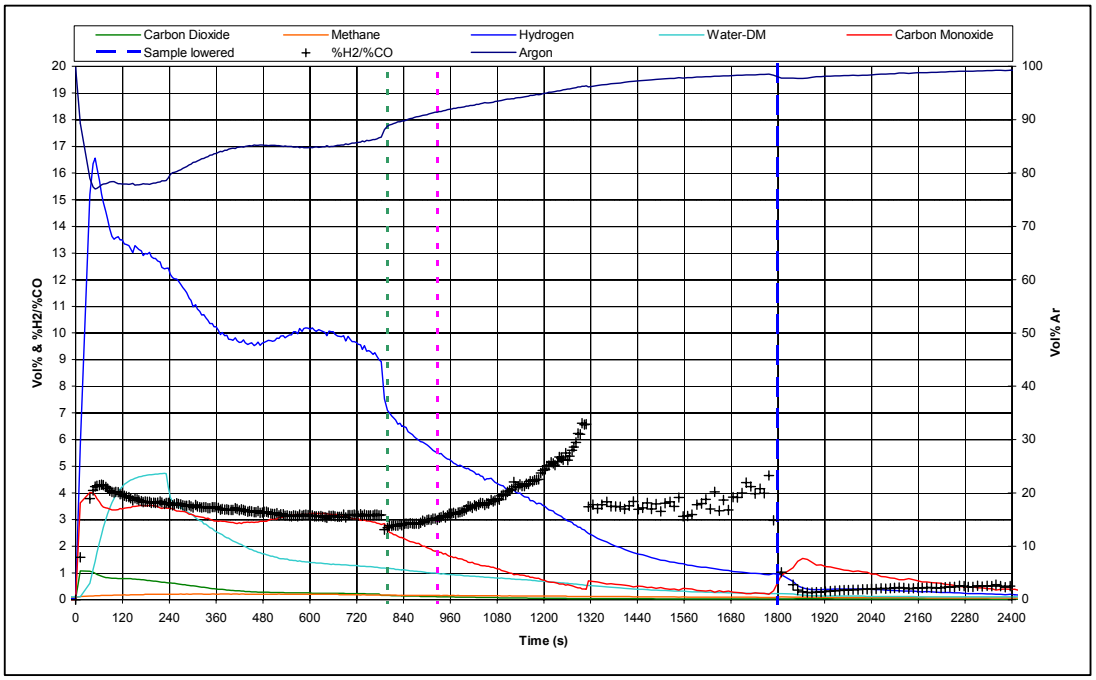

Fig. 46 (a): Coal devolatilisation in coal-alumina sample reacted at 1500°C: Temperatures

(Horisontal temperature lines for reactions (22) to (27) indicates the equilibrium temperatures)

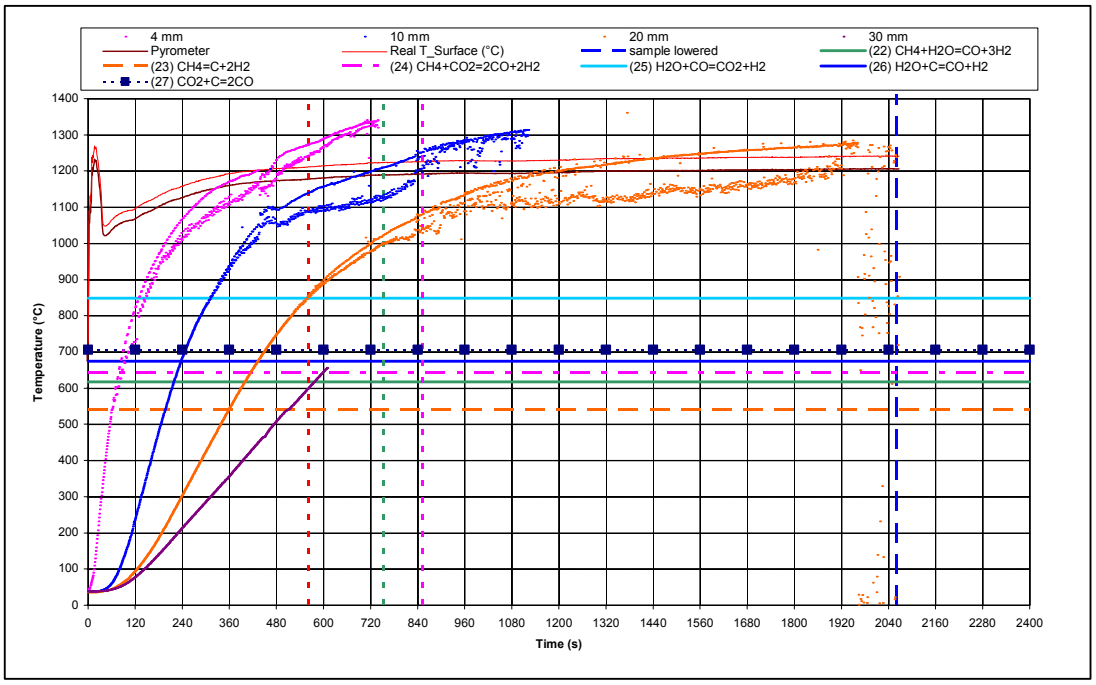

Fig. 46 (b): Coal devolatilisation in coal-alumina sample reacted at 1500°C: Product gas

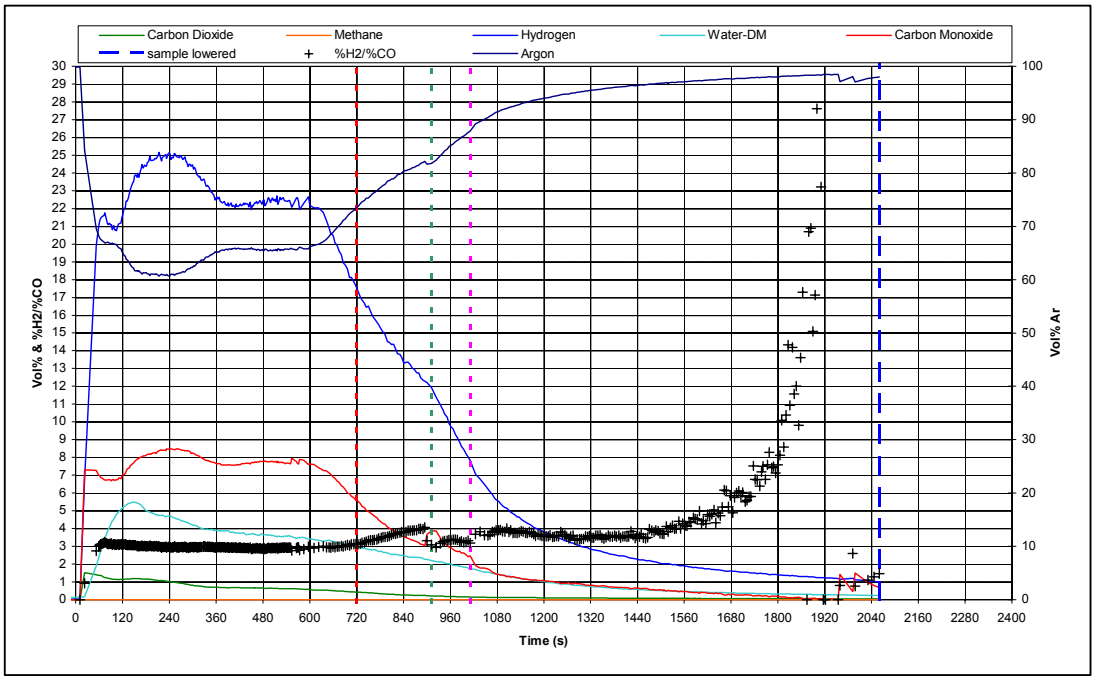

The effect of volatiles on reduction extent has been tested by reaction of char instead of coal as reductant. Comparative sample bed temperatures and product gas analyses are shown for 15 minutes reaction time in **Fig. 47 and 48**. Material bed temperatures in the char containing sample are higher than that for the coal containing sample. The temperature difference can not be uniquely ascribed to the effect of the heat of devolatilisation because the heat of devolatilisation has been found to vary from endothermic to exothermic by 200 kJ/kg parent coal, even for coal of similar composition (Tomeczek and Palugniok, 1996). The difference in material bed temperatures is because of more heat used in reduction work and less heat used to heat up the material layer in the coal containing sample, as compared to a reversal of this heat proportioning in the char containing sample.

The sample surface temperatures for coal containing samples show an apparent increase within the first minute of reaction. This effect is absent when char is used instead of coal. The increased measured temperature is a result of the initial release of volatiles, forming a gas cloud which shielded the radiation seen by the pyrometer, from the sample surface. This was confirmed by video material recorded through an enlarged view hole when a sample of -2000 +1400 µm ore and coal was reacted at 1400°C heating zone one temperature. Snapshots taken from the video material are shown in **Fig. 49**.

Reduction extent for each sample segment is shown in **Fig. 50**, showing that reduction by volatiles does take place for a stagnant bed of material mixture. The composite carbon consumption and reduction levels are shown in **Fig. 51 (a) and (b)**.

Fig. 47: Sample temperatures of Coal vs. Char as reductant

(a) Coal-Ore reacted at 1400°C furnace temperature

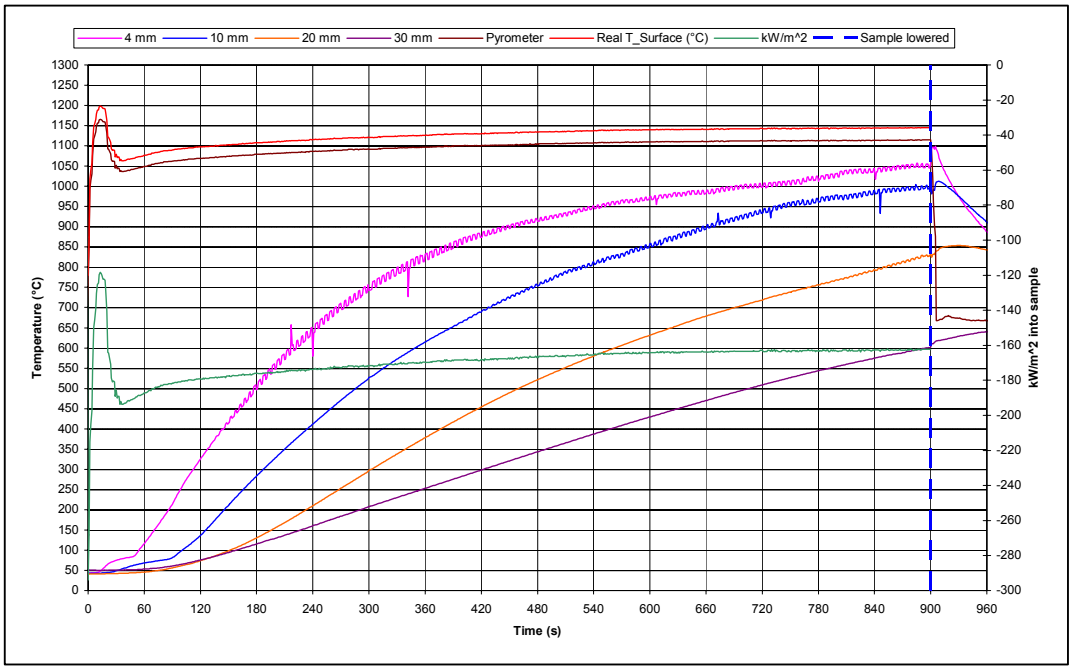

(b) Char-Ore reacted at 1400°C furnace temperature

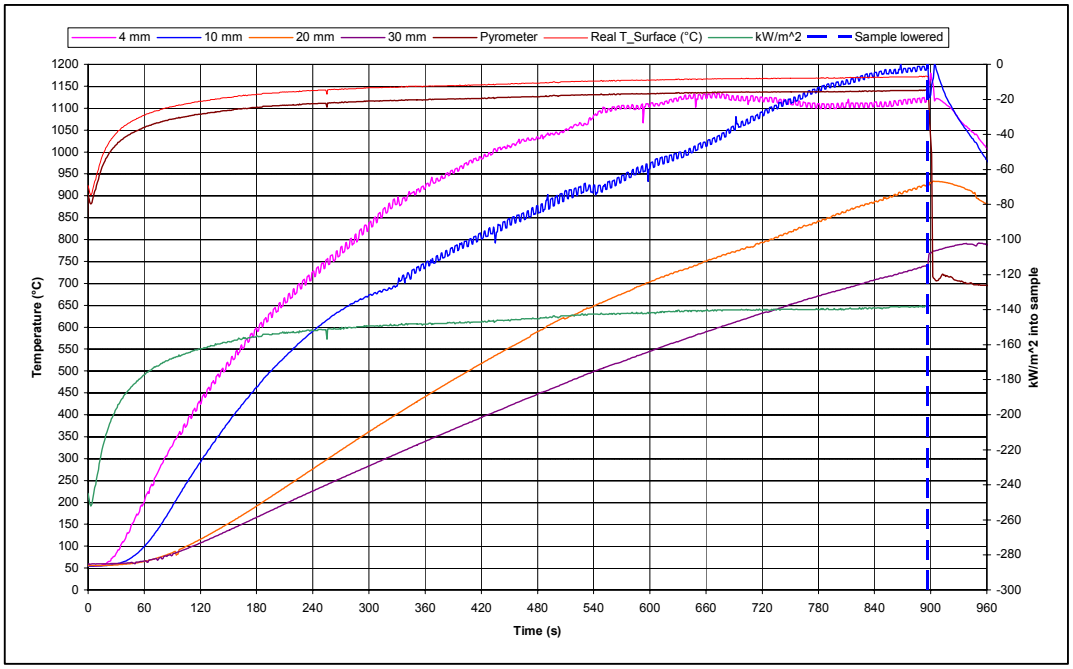

Fig. 48: Product gas for Coal vs. Char as reductant

(a) Coal-Ore reacted at 1400°C furnace temperature

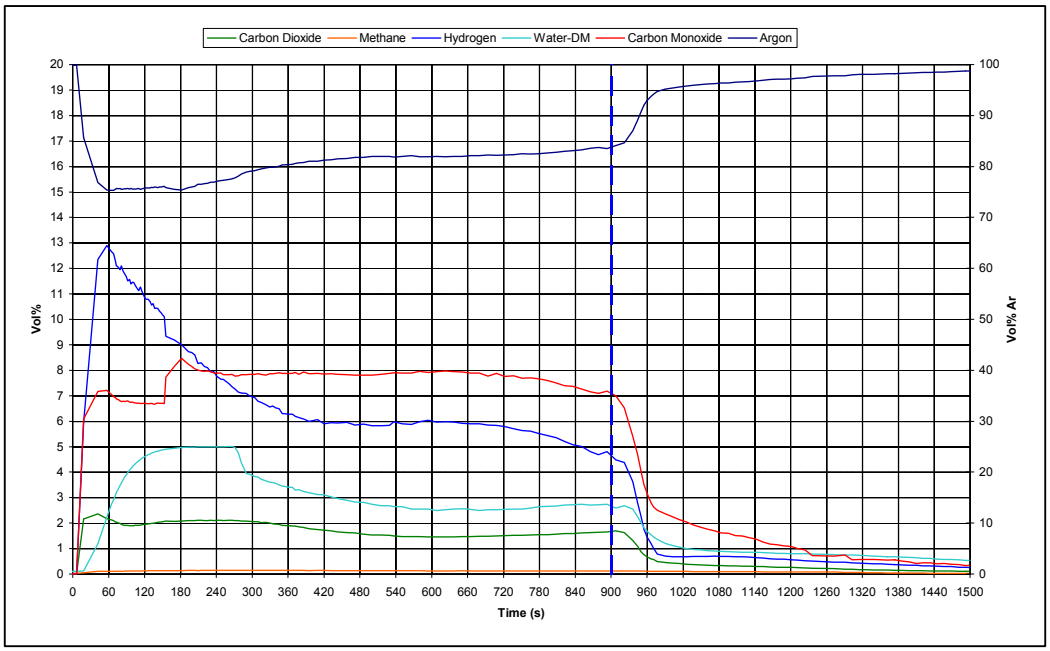

(b) Char-Ore reacted at 1400°C furnace temperature

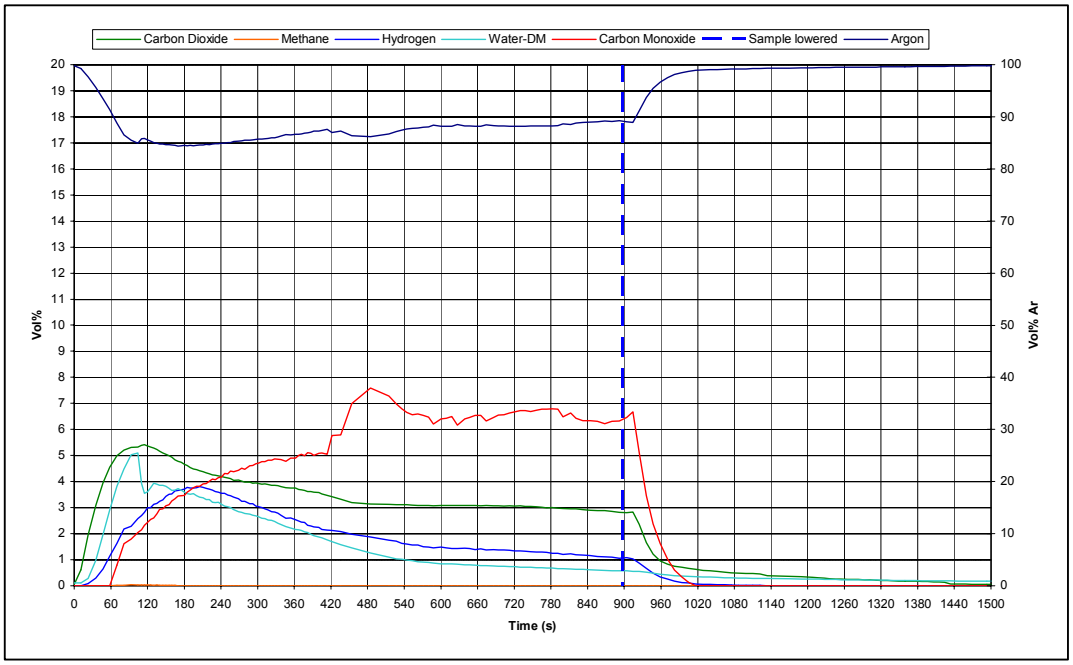

Fig. 49: Snapshots from video material for -2000 +1400 µm ore and coal reacted at 1400°C heating zone1 temperature

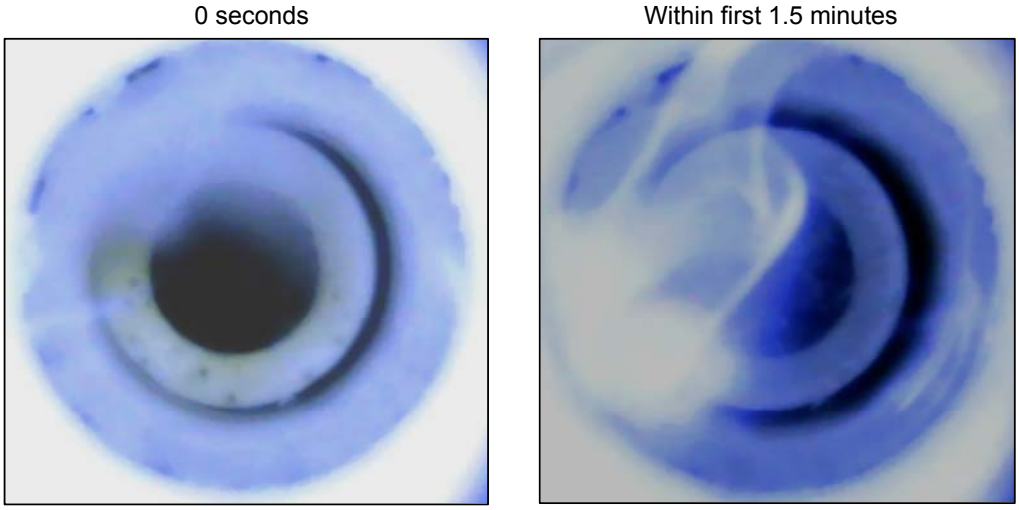

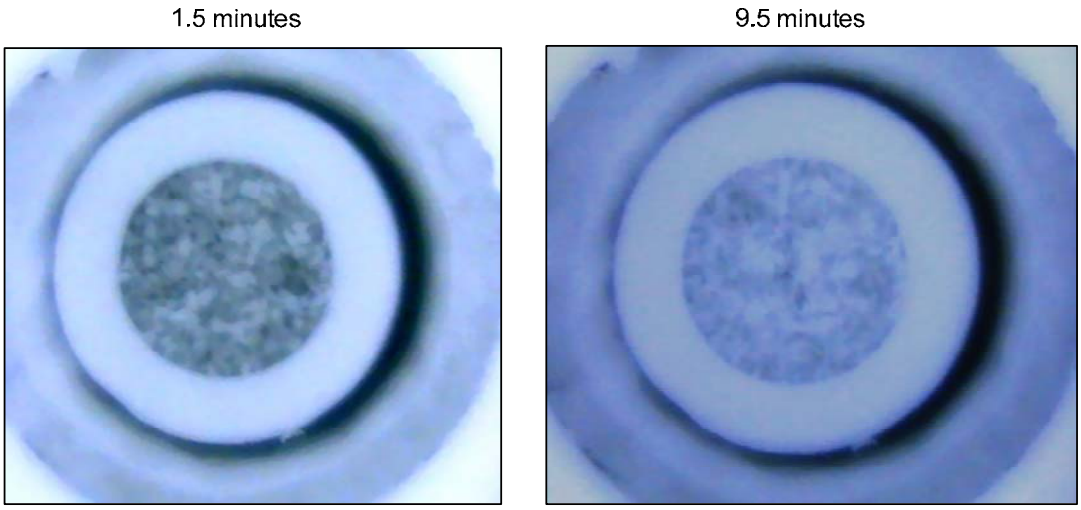

Fig. 50: %Reduction for Coal vs. Char as reductant

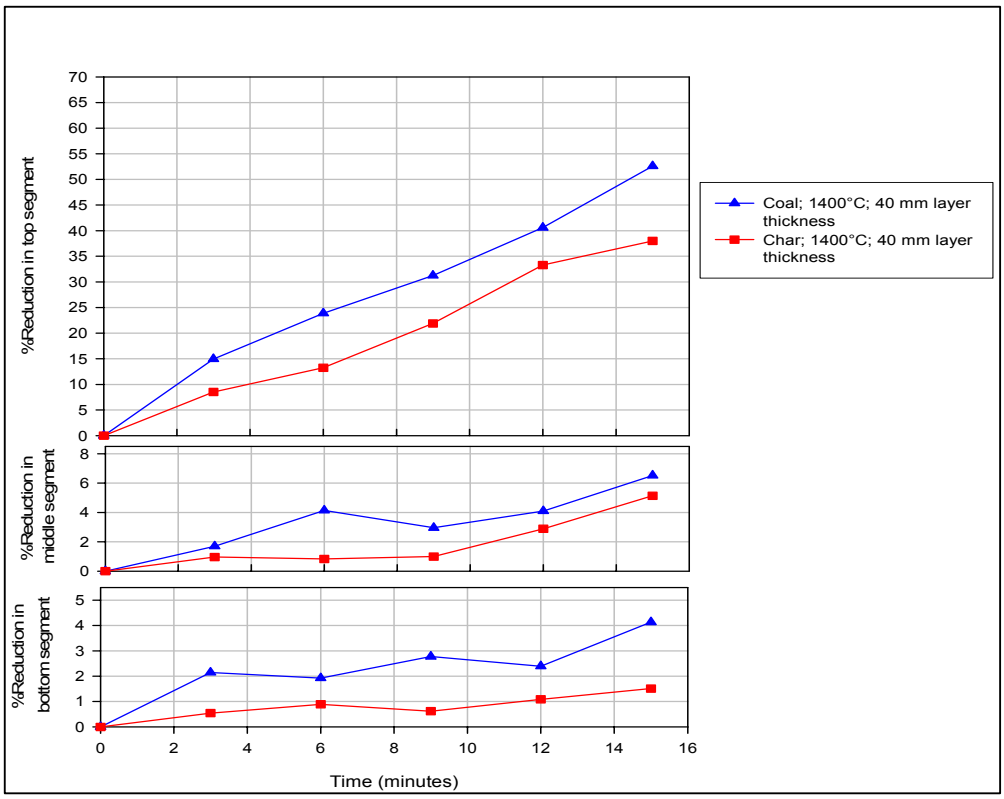

Fig. 51 (a): Composite %Carbon consumption for Coal vs. Char as reductant

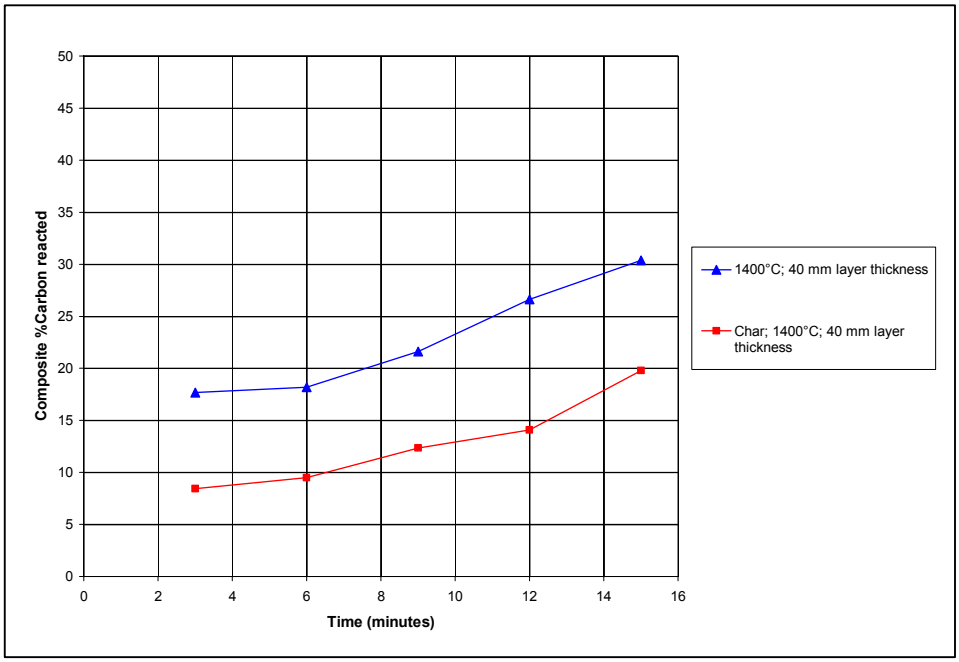

Fig. 51 (b): Composite %Reduction for Coal vs. Char as reductant

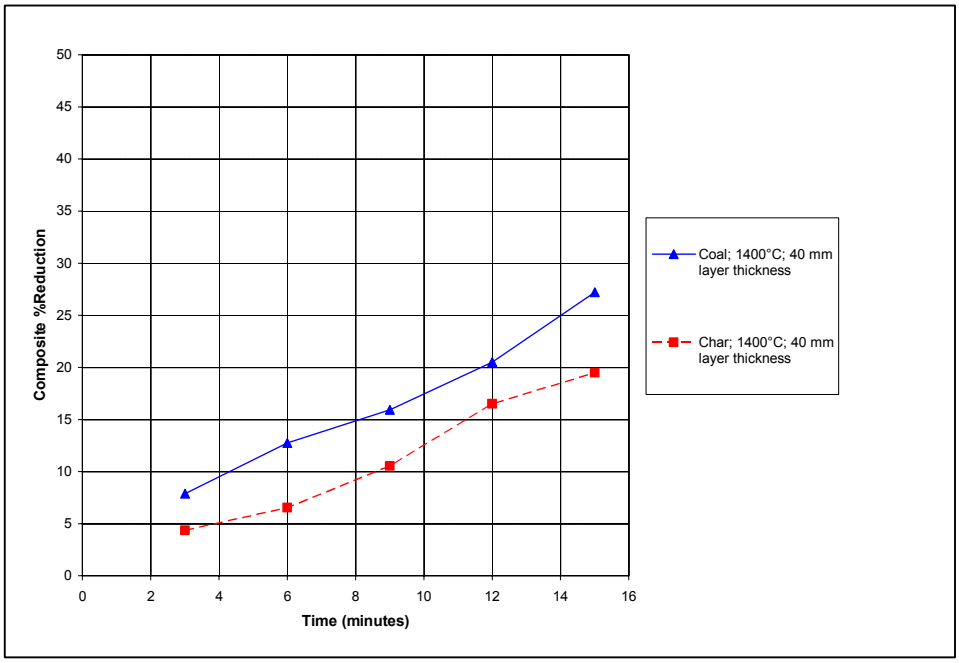

In **Fig. 52** data of the total heat transferred to the sample vs. composite reduction extent is shown. Heat transferred to the coal-ore sample is higher than heat transferred to the char-ore sample, for the same reaction time because the coal-ore sample surface temperatures were lower than that of the char-ore sample surface. The total heat demand in reaction of a coal-ore sample did not exceed the total heat demand for reaction of a char-ore sample to attain the same level of composite reduction. The possible effect of exothermic or endothermic heat of coal devolatilisation on heat transferred to the sample surface is shown as error bars in **Fig. 52**, 200 kJ/kg parent coal (Tomeczek and Palugniok, 1996). The higher reduction extent achieved in the coal-ore samples at equivalent energy input to the sample is most probably because the release of coal volatiles results in more reducing conditions beyond reduction to magnetite in the material layer at lower temperatures, as compared to ~700°C required in the char-ore samples to generate reducing conditions with CO from the gasification reaction. This is in agreement with the work of Sohn and Fruehan (2006b), for a bed of three layers of composite pellets reacted at 1000°C bed surface temperature, which showed significant reduction of the top pellet layer from coal volatiles released from the bottom layer of pellets.

In this study the reduction work done by coal volatiles, primarily hydrogen, released at low material layer temperatures resulted in higher reduction rates in coal-ore samples as compared to char-ore samples. The percentage reduction gain of 4% to 8% for 3 to 15 minutes reaction time was achieved in a stagnant material layer. However, the extent to which this advantage is realised in practice would depend on the process details. For example, if the material is fed through the hot furnace freeboard the coal will devolatilise at least in part and the percentage reduction gain from coal volatiles will be partially reduced, or eliminated. Alternatively the material mixture can be fed to through the furnace sidewalls to gain maximum contribution of coal volatiles in reduction. From the results it is clear that significant reduction by coal volatiles takes place in a mixed coal-ore bed heated uni-directionally from the sample surface. As discussed previously with reference the SL/RN process, in Chapter I, the effect of lowered bed temperature with more reactive reductant used is also observed here for coal vs. char as reductant.

Fig. 52: Total radiation heat transferred vs. Composite %Reduction

(Number inside square frame shows reaction time in minutes)

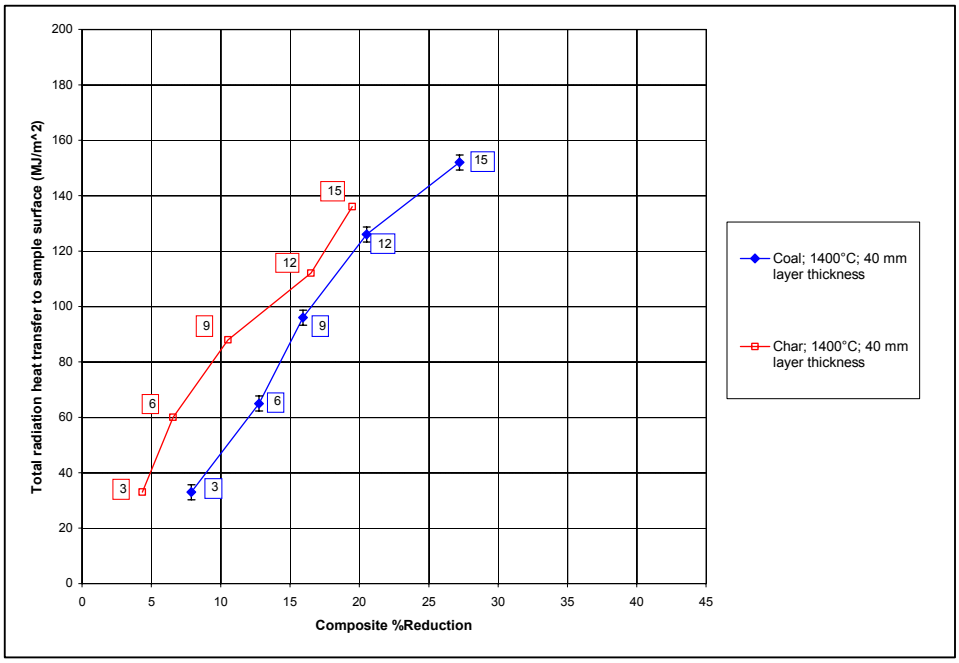

3.5. Phase chemistry of Metal and Oxide Phases

Duplicate samples were reacted for 15 minutes reaction time at 1300°C, 1400°C and 1500°C furnace temperatures and set in epoxy, polished and viewed under reflected light. The photomicrographs taken under reflected light are shown in **Fig. 53 to 55**, and clearly show the variability of reaction of the ore in the top and middle segments. Because the ore contained variable amounts of gangue, and was of variable porosity, ore particles exposed to the same conditions of temperature and reducing atmosphere, showed different degrees of reduction and metallisation. These observations show that this ore does not reduce according to a single rate mechanism. In **Fig. 54 (a)** and **Fig. 55 (a)** extensive metal rim formation is seen around the edge of the reduced ore particle, and the interior is filled with slag and rounded wustite grains. Therefore, the top segment material of the samples reacted for 15 minutes at 1400°C and 1500°C no longer follow exclusively solid state reduction, but are in a semi-molten state. The coal particles also show variable extent of devolatilisation. In **Fig. 55 (b)** some of the coal still has an even texture, whilst the largest coal particle has already reacted somewhat. In the top segment of a sample that has significant metallisation, **Fig. 55 (a)**, the coal has been totally devolatilised, and the carbon skeleton consumed extensively in reduction reactions. The reacted ore and coal features in these photomicrographs clearly show the variability in reaction mechanism for both ore and coal.

The metal product carbon content is important where the aim is to make steel, not hot metal. If the carbon content in the metal product at the heap surface is high, metal refinement is required in the rest of the process zones. The polished sections shown in **Fig. 53-54** were etched with 2% Nital solution to show up the presence of pearlite, indicating carbon content in excess of 0.025%C solubility limit in ferrite. The polished sections were viewed and analysed using a JSM-6300 SEM (Scanning Electron Microscope) at 15 kV and 200 second counting interval. The analysed areas are shown in **Fig. 56-58**. It is seen from the images that no second phase is present in the metal product, indicating that the metal product is ferrite. This is possible because the proximity of carbon to the metal product is not close in the packed bed as seen in **Fig. 53-55**, and there is no carbon deposition onto the metal product. The other interesting observation from the metal analyses is the absence of sulphur, indicating that sulphur pick-up must take place elsewhere in the process.

As is seen from **Fig. 53 (a) and (b)** much variability in reduction is seen for the sample reacted at 1300°C furnace temperature and only a few ore particles were reduced to metal. The metallised ore particles were not restricted to the top segment in the sample. Here two areas with metallised ore particles, in the sample reacted at 1300°C, were analysed for comparison with the analyses of the samples reacted at 1400°C and 1500°C. The ore particle in **Fig. 56 (a)** contained little gangue material and the ore particle is of high porosity so that metallisation occurs throughout the particle and little or no glass phase is formed. In contrast **Fig. 56 (b**) shows metallisation at the ore particle edge and glass phase at the ore particle interior due to high gangue content in the ore particle initially and associated low initial ore particle porosity. Wüstite grains (light grey rounded grains) are embedded in the glass phase. The phase morphology seen in **Fig. 56 (b)** is also seen extensively in the top segments of the samples reacted at 1400°C and 1500°C heating zone 1 temperatures as shown in **Fig. 57** and **Fig. 58**.

Fig. 53 (a): 1300°C furnace temperature; 15 minutes; 40 mm layer, top segment

(C=Coal; O=Ore)

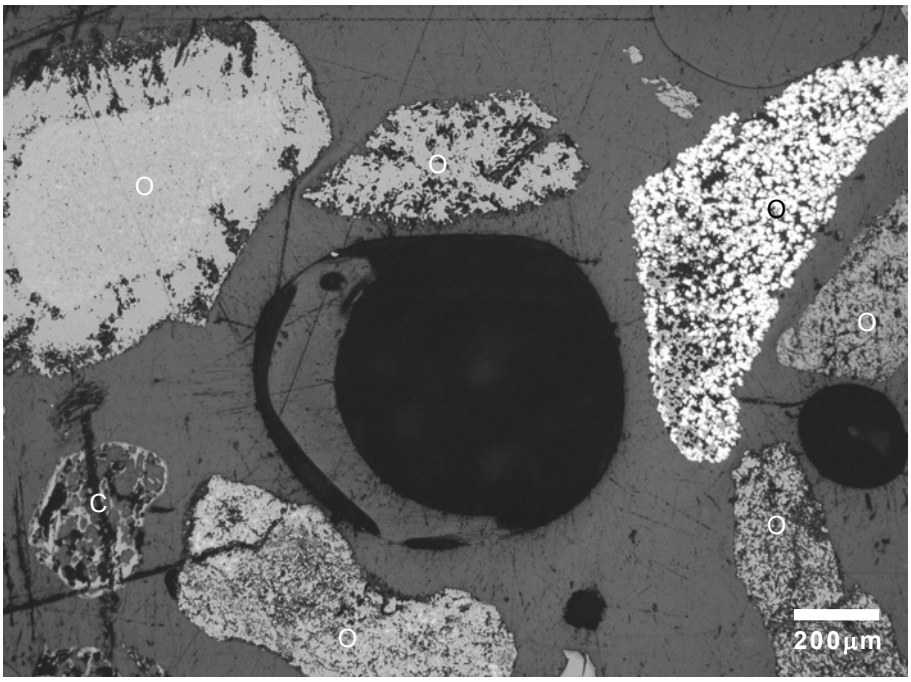

Fig. 53 (b): 1300°C furnace temperature; 15 minutes; 40 mm layer, middle segment

(C=Coal; O=Ore)

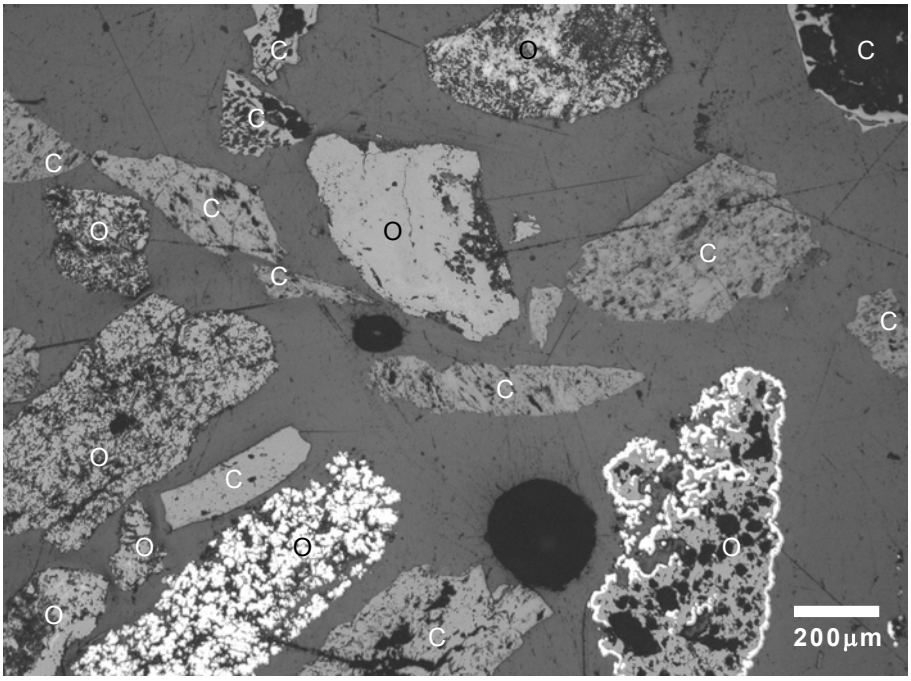

Fig. 54 (a): 1400°C furnace temperature; 15 minutes; 40 mm layer, top segment

(C=Coal; O=Ore)

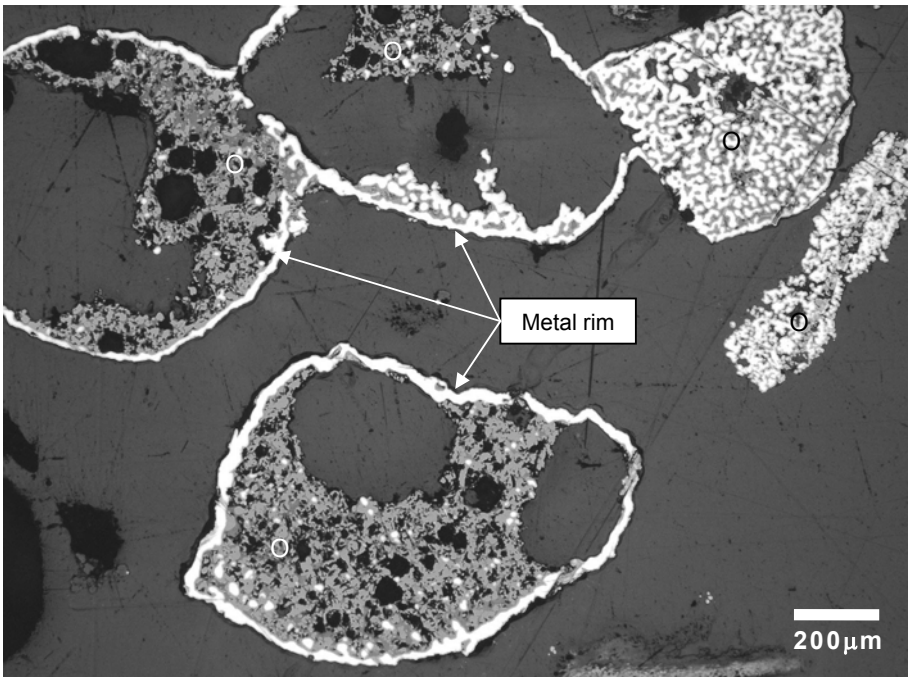

Fig. 54 (b): 1400°C furnace temperature; 15 minutes; 40 mm layer, middle segment

(C=Coal; O=Ore)

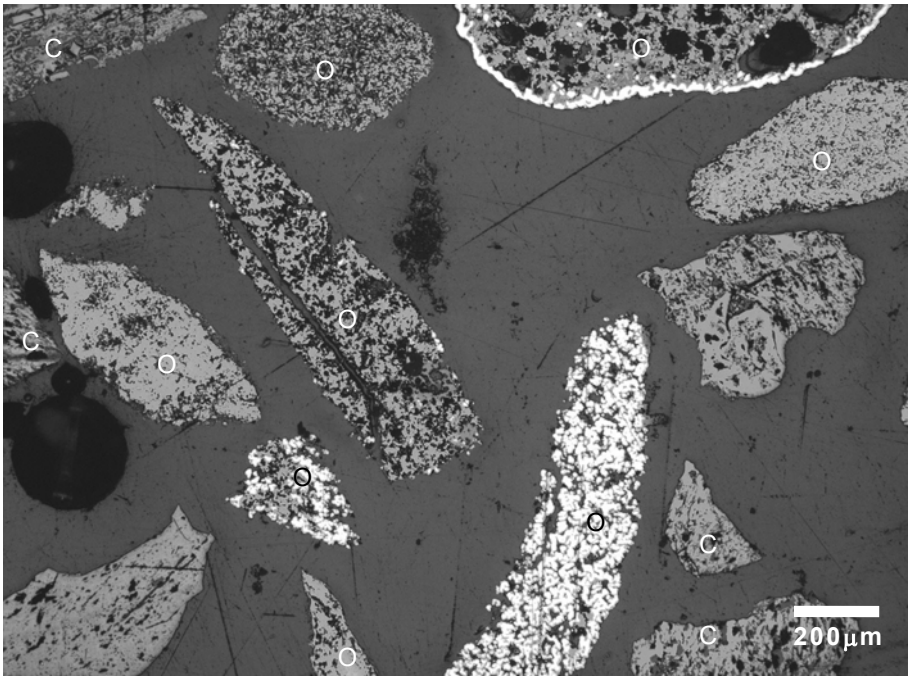

Fig. 55 (a): 1500°C furnace temperature; 15 minutes; 40 mm layer, top segment

(C=Coal; O=Ore)

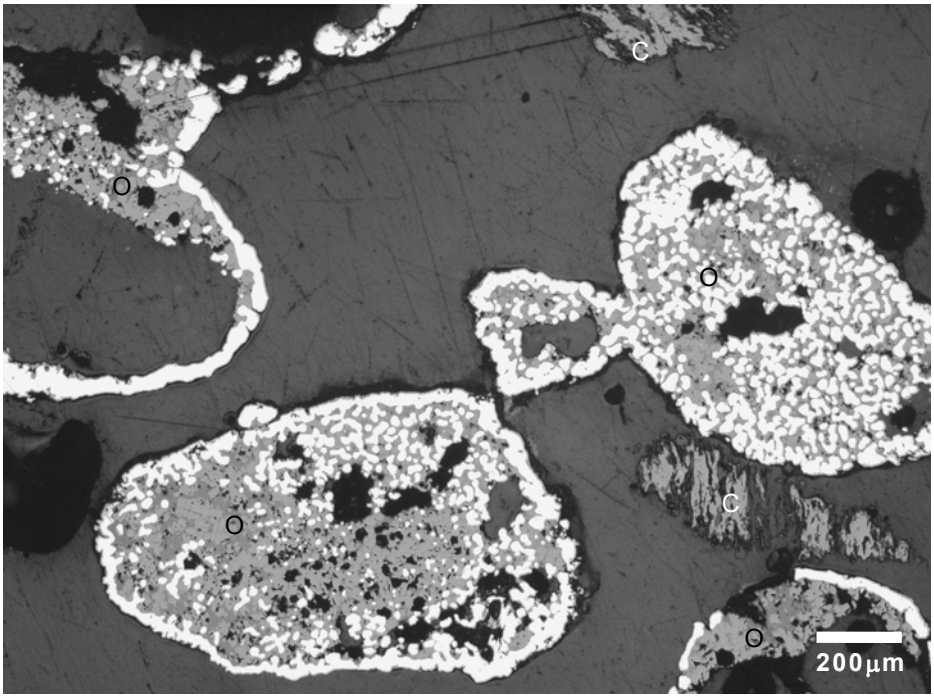

Fig. 55 (b): 1500°C furnace temperature; 15 minutes; 40 mm layer, middle segment

(C=Coal; O=Ore)

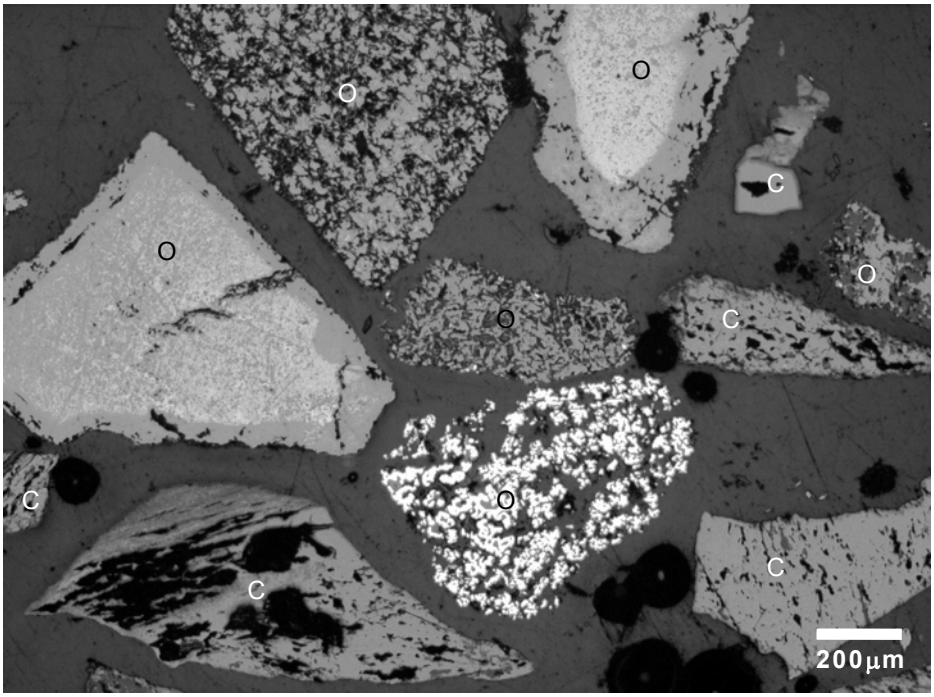

The analyses from **Fig. 58 (a)** show that the oxide phases consist of FeO (light grey rounded grains) and silicate needles initially. The composition of the needles corresponds to the stoichiometry for Fayalite, $2FeO.SiO_2$, with a liquidus temperature of 1208°C and solidus temperatures of 1175°C associated with FeO, and 1180°C associated with silica. The sample surface temperature is ~ 1250°C whilst the sample bed temperature 10 mm from the sample surface is ~ 1160°C. Therefore, the silicate phase could have been liquid at the sample temperatures, but not the FeO areas because the lowest solidus temperature for FeO is 1371°C. This is important because the lowered oxide liquidus temperature limits the maximum temperature to which the heap surface can be heated without bulk melting. This is a function of the gangue component in the ore so that use of a higher quality ore will allow for higher heap surface temperatures. The silicate glass composition changes from higher FeO content initially to lower FeO content as the FeO grains are reduced. The lower FeO content in the silicate glass is seen from **Fig. 58 (b)**. As shown in **Fig. 57 (a) and (b)**, similar phase morphology is seen in the top segment of the sample reacted for 15 minutes at 1400°C. The glass phase analyses shown in **Fig. 56 (b)**, **Fig. 57 (a) and (b)** and **Fig. 58 (b)** are all similar in composition to the silicate needles' composition in **Fig. 58 (a)** with the stoichiometry of Fayalite, $2FeO.SiO_2$. However, the material layer surface temperatures were 1084°C, 1145°C and 1256°C for the samples reacted at heating zone 1 temperatures of 1300°C, 1400°C and 1500°C. The liquidus temperature of Fayalite is 1208°C and the solidus 1175°C. Melting of Fayalite could only take place at 1084°C and 1145°C because of the presence of Fe^{3+} in the Fayalite and/or substitution of minor elements such as K, Na, P into the glass phase to reduce the liquidus and solidus temperature. The partial oxygen pressures for the CO/CO_2 values were calculated at the sample surface temperatures of 1084°C, 1145°C and 1256°C to be 4×10^{-12}, 3×10^{-11} and 2×10^{-9} atm. At these partial oxygen pressures Fe^{3+} should be present in the glass phase. Glass phase formation within ore particles should be avoided as it results in decreased porosity resulting in metallisation restricted to the glass phase boundary, as seen above. Furthermore, bulk melting of ore should be avoided because energy utilisation is shifted toward melting rather than reduction and metallisation at the heap surface.

Fig. 56 (a): Phases in Top segment of coal-ore sample reacted at 1300°C for 15 minutes

(Right hand image is area in blue block enlarged)

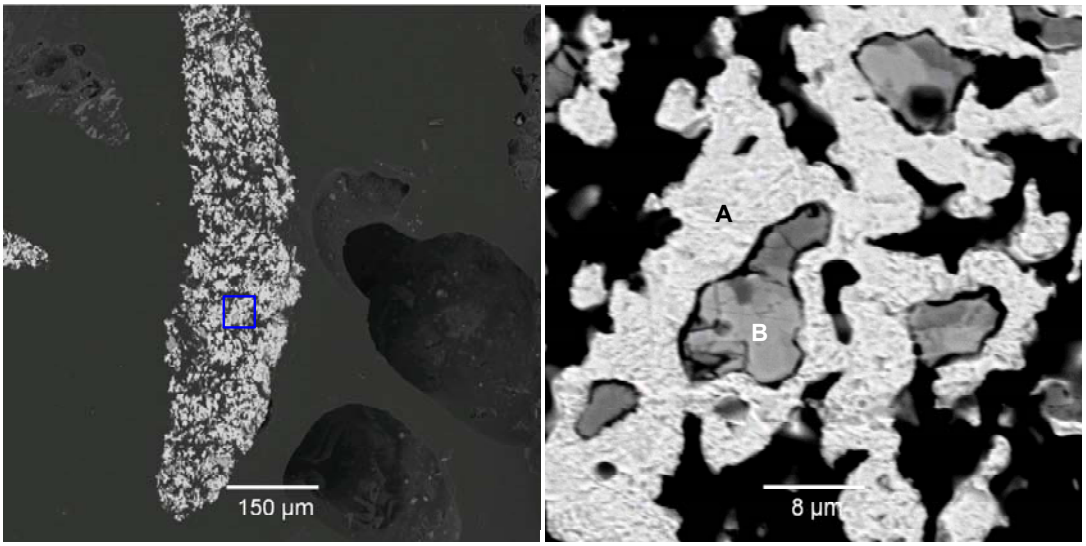

Element	Fe	Si	Al	Ca	K	Ba	Ti	Mg	Mn	S	P	Na	Total
A: Metal (mass%)	99.6	0.0	0.0	0.1	0.1	0.1	0.0	0.1	0.0	0.0	0.0	0.0	100
B: FeO grains (mass%)	95.6	0.7	3.2	0.0	0.0	0.0	0.0	0.0	0.0	0.2	0.0	0.1	100

Fig. 56 (b): Phases in Top segment of coal-ore sample reacted at 1300°C for 15 minutes
(Right hand image is area in blue block enlarged)

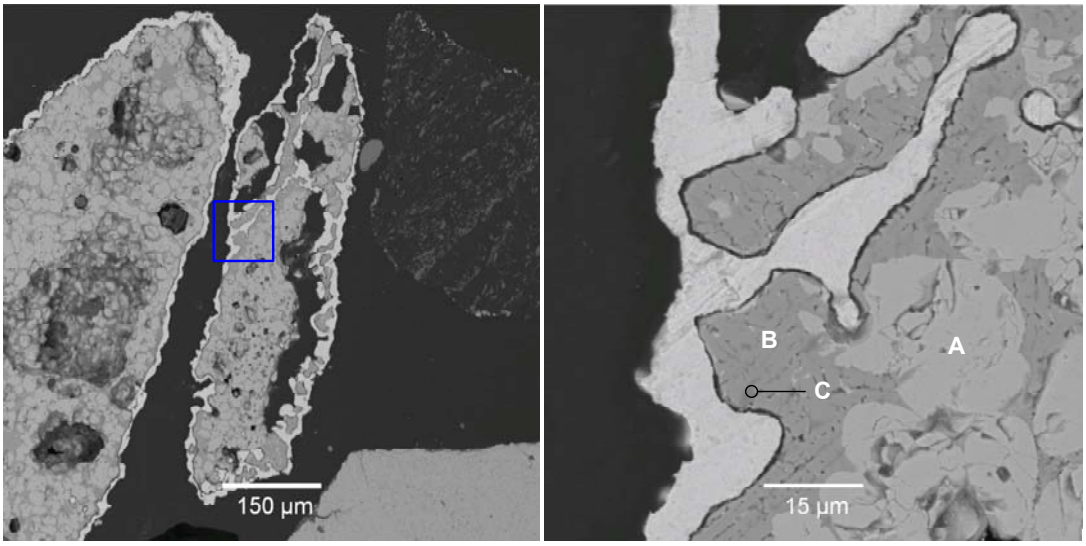

Element	Fe	Si	Al	Ca	K	Ba	Ti	Mg	Mn	S	P	Na	Total
A: FeO grains (mass%)	98.6	0.3	0.7	0.0	0.0	0.0	0.0	0.2	0.0	0.1	0.0	0.0	100
B: Glass (mass%)	75.5	16.9	3.3	1.6	0.2	0.6	0.0	0.1	0.3	0.7	0.8	0.0	100
B: Glass (mol fraction)	0.62	0.28	0.06	0.02	0.00	0.00	0.00	0.00	0.00	0.01	0.01	0.00	1.00
C: Dark phase (mass%)	70.4	10.9	17.0	0.4	0.1	0.0	0.2	0.0	0.3	0.1	0.5	0.2	100

Fig. 57 (a): Phases in Top segment of coal-ore sample reacted at 1400°C for 15 minutes
(Right hand image is area in blue block enlarged)

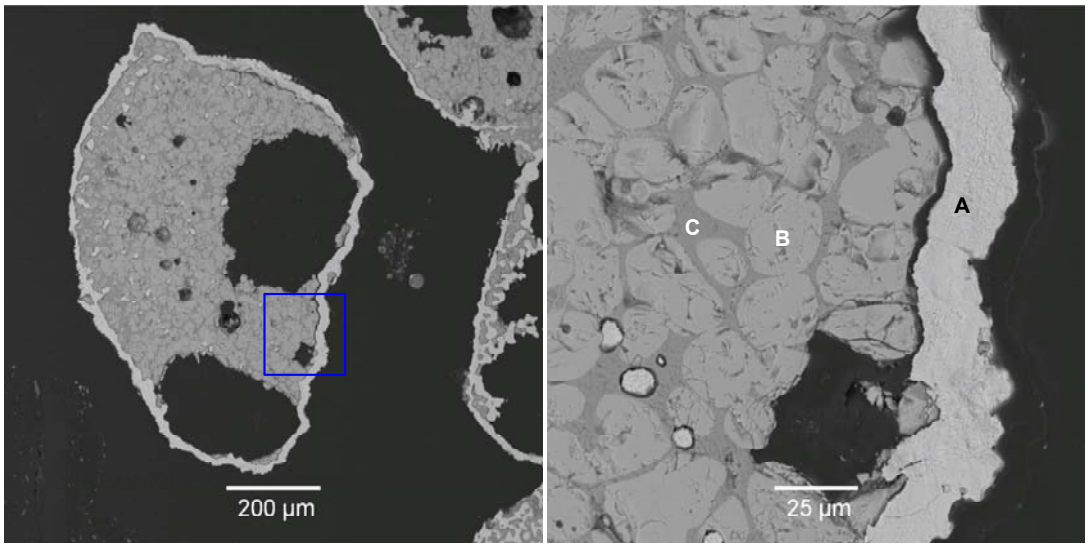

Element	Fe	Si	Al	Ca	K	Ba	Ti	Mg	Mn	S	P	Na	Total
A: Metal (mass%)	99.4	0.2	0.2	0.1	0.1	0.0	0.0	0.0	0.0	0.1	0.0	0.0	100
B: FeO grains (mass%)	98.0	0.3	1.0	0.1	0.0	0.0	0.2	0.1	0.2	0.0	0.0	0.1	100
C: Glass (mass%)	77.9	13.4	6.0	0.4	0.2	0.3	0	0.2	0.1	0.7	0.6	0.1	100
C: Glass (mol fraction)	0.64	0.22	0.10	0.00	0.00	0.00	0.00	0.00	0.00	0.01	0.01	0.00	1.00

Fig. 57 (b): Phases in Top segment of coal-ore sample reacted at 1400°C for 15 minutes
(Right hand image is area in blue block enlarged; black blocks = analysed area)

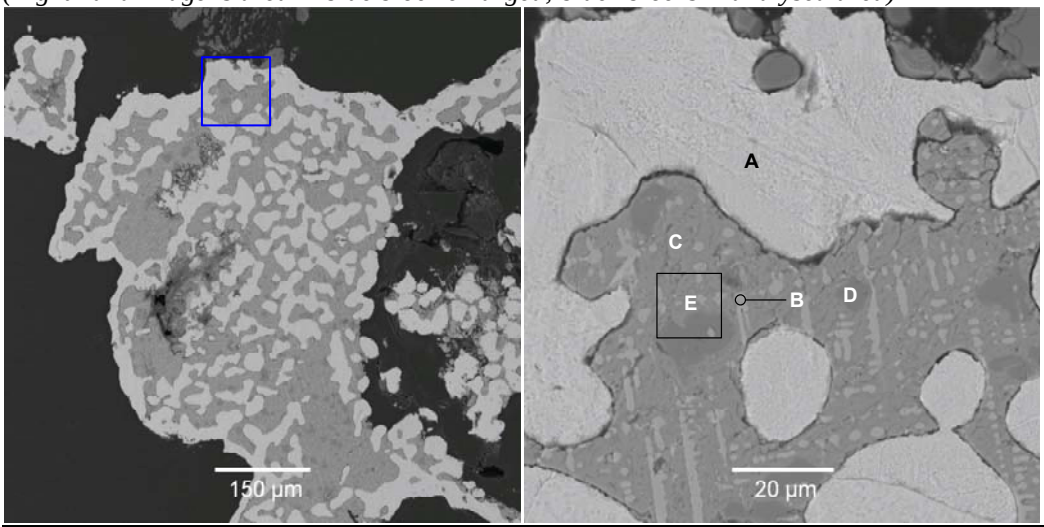

Element	Fe	Si	Al	Ca	K	Ba	Ti	Mg	Mn	S	P	Na	Total
A: Metal (mass%)	99.6	0.1	0.1	0.0	0.0	0.1	0.0	0.0	0.0	0.1	0.0	0.0	100
B: FeO dendrites (mass%)	94.1	2.4	2.4	0.1	0.0	0.2	0.2	0.0	0.0	0.5	0.0	0.2	100
C: Glass (mass%)	77.0	17.2	3.3	0.5	0.1	0.2	0.2	0.1	0.0	0.8	0.5	0.0	100
C: Glass (mol fraction)	0.63	0.28	0.06	0.01	0.00	0.00	0.00	0.00	0.00	0.01	0.01	0.00	1.00
D: Dark phase (mass%)	64.9	4.7	28.5	0.1	0.1	0.4	1.1	0.0	0.0	0.2	0.0	0.0	100
E: Oxide area analysis (mass%)	79.1	12.8	4.9	0.4	0.2	0.0	0.3	0.0	0.0	1.6	0.3	0.2	100

Fig. 58 (a): Phases in Top segment of coal-ore sample reacted at 1500°C for 15 minutes
(Right hand image is area in blue block enlarged)

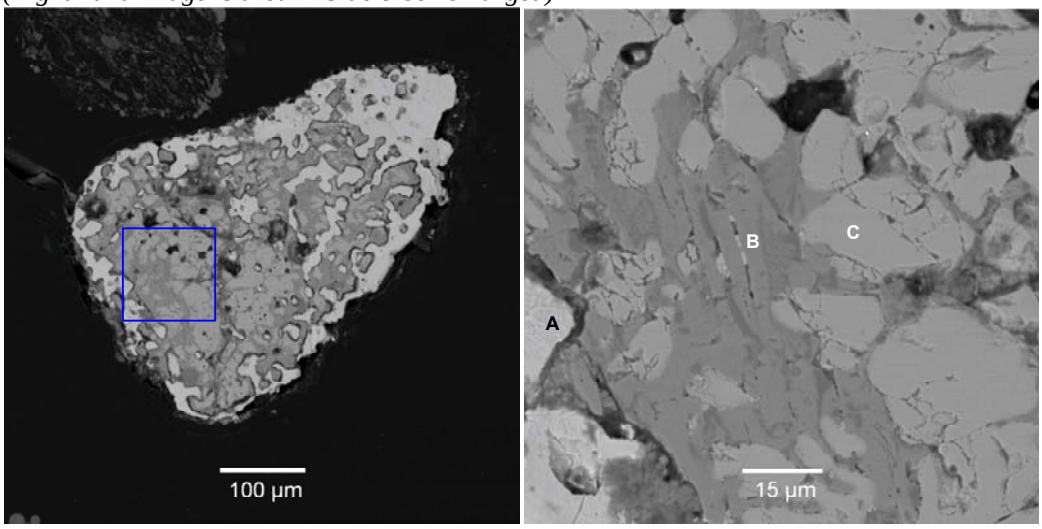

Element	Fe	Si	Al	Ca	K	Ba	Ti	Mg	Mn	S	P	Na	Total
A: Metal (mass%)	99.8	0.1	0.1	0	0	0	0	0	0	0	0	0	100
B: Needles (mass%)	79.0	18.9	0.5	0.8	0.1	0	0	0	0.1	0	0.4	0.1	100
C: FeO grains (mass%)	98.2	0.3	0.9	0	0	0	0.1	0	0.2	0	0	0.2	100
B: Needles (mol fraction)	0.66	031	0.01	0.01	0.00	0.00	0.00	0.00	0.00	0.00	0.01	0.00	1.00

Fig. 58 (b): Phases in Top segment of coal-ore sample reacted at 1500°C for 15 minutes
(Right hand image is area in blue block enlarged; black blocks = analysed area)

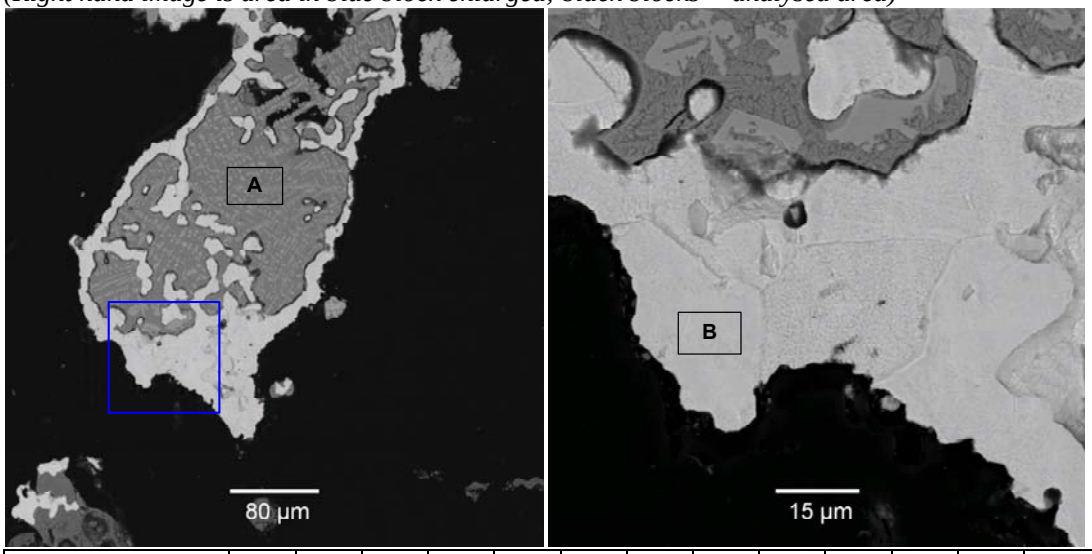

Element	Fe	Si	Al	Ca	K	Ba	Ti	Mg	Mn	S	P	Na	Total
A: Glass (mass%)	61.8	19.9	5.8	0.8	0.3	0.0	8.8	0.7	0.5	1.1	0.2	0.2	100
A: Glass (mol fraction)	0.48	0.30	0.09	0.01	0.00	0.00	0.08	0.01	0.00	0.01	0.00	0.00	1.00
B: Metal (mass%)	99.2	0.3	0.2	0.0	0.0	0.0	0.0	0.1	0.1	0.0	0.1	0.0	100

3.6. Effect of particle size

The effect of particle size fraction was tested to gauge the relative importance of the reduction reaction and the gasification reaction, respectively. The basis size fraction of -850 +425 µm was used for ore and coal particles. For particle size fraction testing the coal in the mixture was changed to a smaller size fraction of -425 +300 µm and a larger size fraction of -2000 +1400 µm, respectively whilst using the ore of the basis size. The same variation in ore particle size was used in combination with the basis size fraction coal. The samples were reacted at 1400°C furnace temperature for 9 minutes reaction time. The variation in reduction extent and carbon consumption are summarised in **Table 14**.

Table 14: Effect of particle size variation at 1400°C and 9 minutes for 40 mm layer material

Sample Change	Ore size fraction (µm)	Coal size fraction (µm)	Composite %R*	Top Segment %R*	%C consumption	Top Segment %C consumption	Average kW/ m^2
Coarse Ore	-2000 +1400	-850 +425	17	33	27	36	-152
Coarse Coal	-850 +425	-2000 +1400	15	25	22	41	-146
Fine Coal	-850 +425	-425 +300	21	40	28	53	-153
Fine Ore	-425 +300	-850 +425	23	44	23	39	-153
Basis	-850 +425	-850 +425	16	31	22	30	-178

%R = %Reduction

The product gas reducing potential is shown in **Fig. 59**. Heat transferred to the sample as a function of composite reduction extent is shown in **Fig. 60**. The energy input into the samples with larger and smaller particles are similar in magnitude, and the energy input values of this group is lower than that of the basis case. Although the energy input among the particle size variation samples is similar the reduction extent in the top node of these samples differs significantly. Different product gas temperature may result from different particle size material reacted (for example, if the mixture is more reactive, reaction can occur at a lower temperature, leading to a lower bed temperature and hence a lower off-gas temperature). To quantify the possible effect of different product gas temperature on the total heat transfer to the sample (as required for reduction), a simple heat-mass balance was used to calculate the heat input to the sample with product gas temperature variation of ±100°C. The resultant variation in total heat transfer was ±3 MJ/m^2. This is small compared with the differences in heat transferred (for similar degrees of reduction) for the beds of different particle sizes (see **Fig. 60**).

A clear increase in reduction extent is seen when smaller ore or coal particles are reacted, as compared to reaction of larger ore and coal particles. Increased reduction extent achieved for decreased particle size is most likely due to decreased diffusion barriers to reacting gases in the case of reduction and gasification. Alternatively, reduced particle sizes may reduce the effect of diffusion barriers as a result of increased surface area of reacting particles. The presence of diffusional barriers to reduction gasses as a result of glass phase formation was shown in **Fig. 54** and **Fig. 57**. Variable gasification extent of

char particles in close proximity is also seen in **Fig. 54 (b)**; compare the char particle in top left hand corner with the char particle in bottom left hand corner. Increased reduction rates for smaller coal and ore particles indicate that the reduction reaction and the gasification reaction in combination are important. The increased reduction extent for fine coal and fine ore is confirmed from the higher reducing potential in the product gas as shown in **Fig. 59**. Carbon consumption differences are significant in the top node, but explanation of the relative differences is complicated by the effect of devolatilisation gases in reduction on the overall carbon consumption. Increased ore particle size does not result in significant change in reduction extent, whilst increased coal particle size results in decreased reduction extent, confirming the importance of diffusion effects on the reduction reaction.

Fig. 59: %CO/(%CO+CO_2) in product gas: 9 minute reaction time at 1400°C furnace temperature for 40 mm material layer and different particle sizes

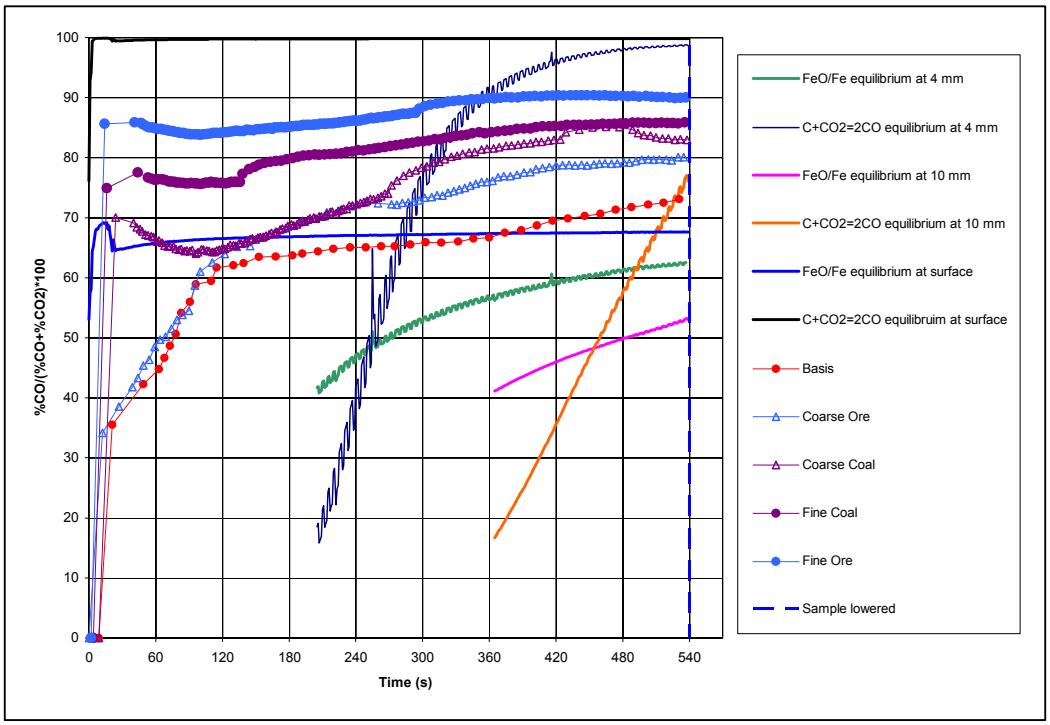

Fig. 60: Total radiation heat transferred vs. Composite %Reduction

(Number inside square frame shows reaction time in minutes)

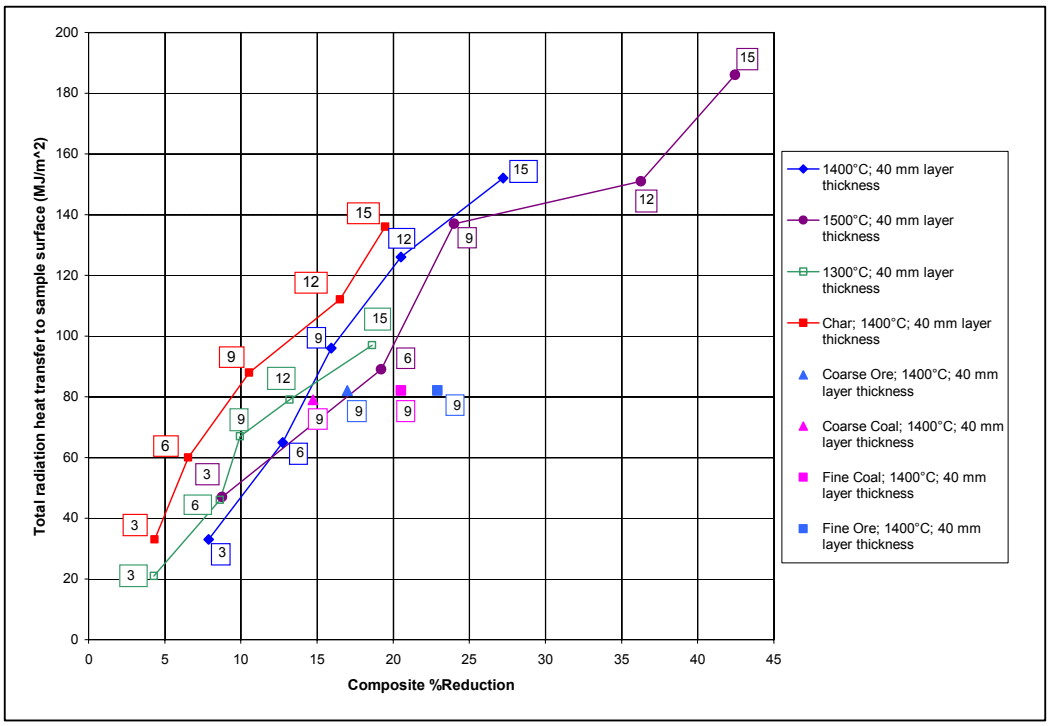

Comparison for material layer temperatures for fine and coarse ore and coal particle sizes is shown in **Fig. 61 (a) and (b)**. Except for the material layer temperatures at 10 mm from the sample surface, the temperatures for fine and coarse ore particle sizes in the samples are similar. For variation in coal particle size it is clear from **Fig. 61 (b)** that material layer temperatures are lower in the case of fine coal as compared to coarse coal. This temperature difference indicates increased energy use for reaction of the sample rather than heating the sample, in agreement with higher reaction extents for smaller sized particles as shown in **Table 14**.

Fig. 61 (a): Material layer temperatures for fine and coarse ore particles

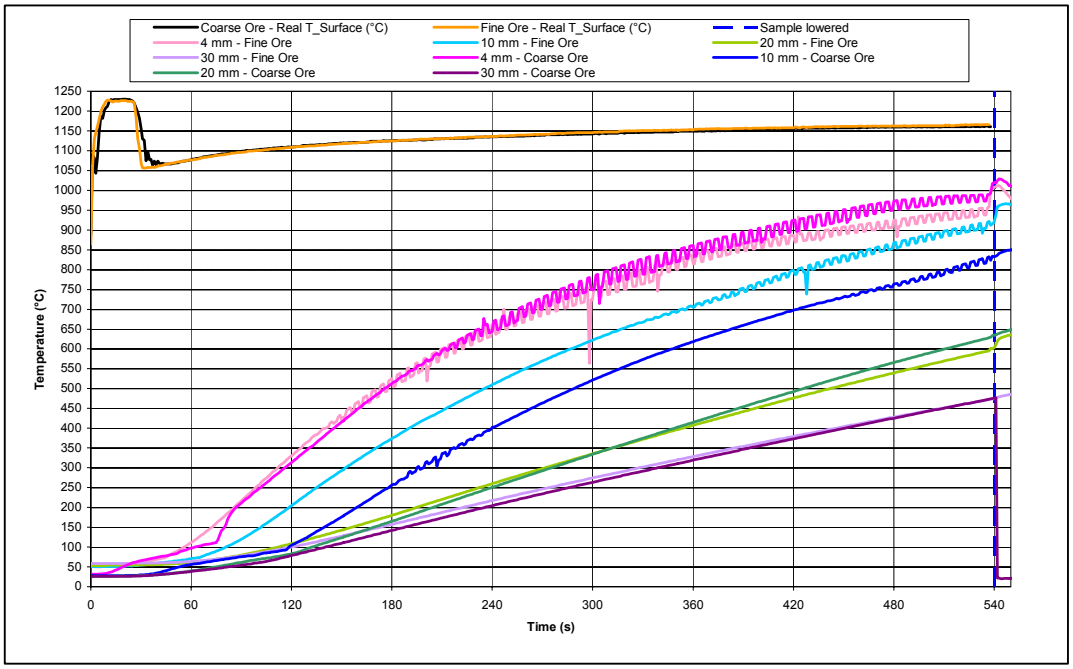

Fig. 61 (b): Material layer temperatures for fine and coarse coal particles

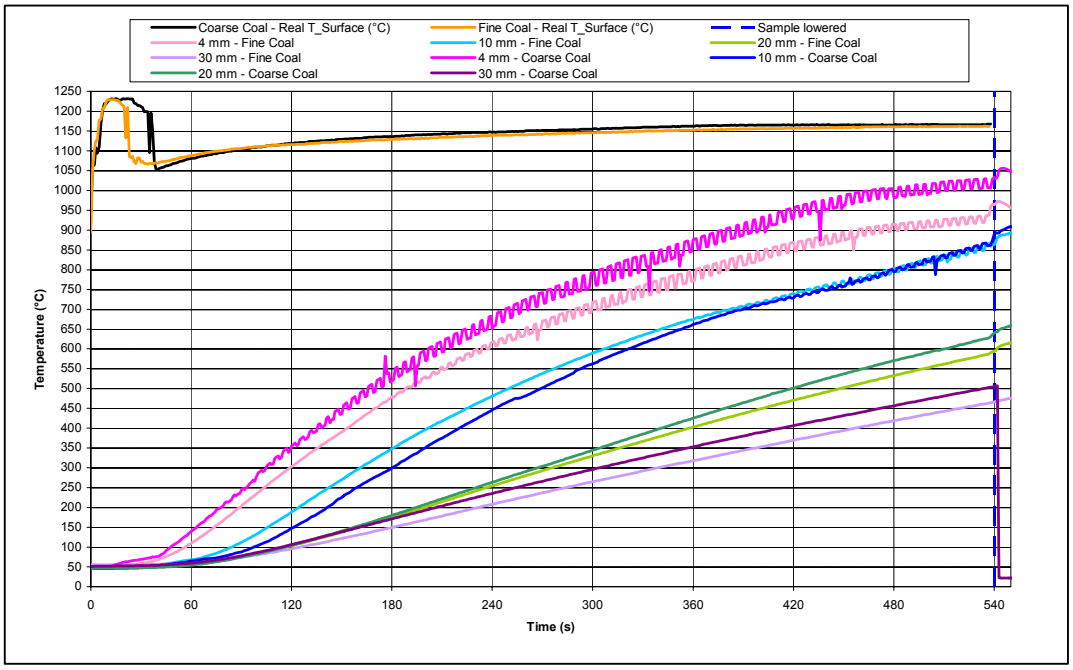

The input sample bulk densities were of similar magnitude (1391-1423 kg/m^3), indicating that initial particle packing density could not influence heat transfer within the sample by changing the material bed conductivity. Some bed compaction should take place as a result of reduction to improve the conductivity of the material bed. In addition metallisation in the top segment can also increase conductivity in the material bed. Differences between the endpoint temperatures measured at respective positions in the material layer are shown in **Table 15**. The difference in material layer temperatures for fine ore and fine coal are of similar magnitude, and that for coarse ore and coarse coal is similar. This indicates similarities in heat transfer effects within the material layer when mixtures of fine ore and coal, respectively, were reacted. The latter effect may be due to similar extent of reduction and metallisation for fine ore and coal to improve material bed conductivity.

Table 15: Material bed temperatures for coarse and fine ore/coal particle size material reacted at 1400°C and 9 minutes, 40 mm material layer

Sample Change	*Surface	*4 mm	*10 mm	*20 mm	*30 mm	[2]Surface – 4 mm	[2]4 mm – 10 mm	[2]10 mm – 20 mm	[2]20 mm – 30 mm
Coarse Ore	1161	992	823	629	474	169	169	194	155
Coarse Coal	1167	1006	862	631	503	161	144	231	128
Fine Coal	1161	937	866	588	464	224	71	278	124
Fine Ore	1166	958	921	596	472	208	37	325	124

*Temperature at indicated material layer position. [2] Temperature difference between material layer temperatures measured at indicated positions.

3.7. Conclusions and Future Work

- The simulation experiment developed in this work adequately quantifies radiation heat transfer to a material layer heated uni-directionally from the sample surface. These results show the importance of heat transfer in the IFCON® process.

- Radiative and conduction heat transfer control prevails for 16 mm to 40 mm material layers heated uni-directionally from the material layer surface. Radiative heat transfer control is indicated by the persistent temperature differential measured between the sample surface and the furnace heating zone temperatures and increased reaction extent achieved with increased radiation heat transfer to the sample surface. At 1400°C furnace temperature the temperature differentials between the main radiation heat source, heating zone at 1410°C, and the sample surface temperatures were 266-303°C for 40 mm material layers, and 240-287°C for 16 mm material layers. Conduction heat transfer control is indicated by the persistent temperature differentials within the material layer measured after initial heating of the material layer. Increased reaction extent for decreased material layer thickness confirms conduction heat transfer control in the material layer. At 1400°C furnace temperature the temperature differentials between the material layer surface temperature and the material layer bottom temperatures were 543-995°C for 40 mm material layers, and 914-105°C for 16 mm material layers. At 15 minutes reaction time of a 16 mm layer the temperature differentials within the material layer were eliminated.

- Coal volatiles contribute to reduction in a 40 mm layer material bed, mainly in the form of hydrogen. Some CO and CO_2 are also released as volatile material at higher material bed temperatures.

- The product gas for the coal-ore material layers reacted non-isothermally in this work is of sufficiently high reducing potential to reduce FeO to Fe, even from the start of reaction when only the sample surface is at high temperature. The product gas analyses follow a reducing potential between that of the FeO/Fe and the C/CO_2 equilibrium values.

- Reduction of Sishen fine ore does not follow a single reaction mechanism because of variability of gangue content and porosity in the ore grains. The metal product formed is ferrite. Glass phase of Fayalite ($2FeO.SiO_2$) stoichiometry was formed. Therefore reduction did not follow exclusively solid state reduction, but reduction occurred in a semi-molten state. The lowered oxide liquidus temperature, compared to that of FeO, limits the maximum temperature to which the heap surface can be heated without bulk melting, and so sets a limit to radiation heat transfer rates which are practically attainable.

- Increased ore size fraction from -850 +425 µm to -2000 +1400 µm, did not result in significant change in reduction extent and carbon consumption. However a clear increase in reduction extent and carbon consumption was seen when a reduced ore size fraction of -425 +300 µm was reacted. Increased reduction extent and increased carbon consumption were observed when a reduced coal size fraction of -425 +300 µm (from -850 +425 µm) was reacted. For increased coal size fraction to -2000 +1400 µm reduction extent decreased and carbon consumption increased. Increased reaction rates for smaller coal and ore particles are most likely due to decreased diffusion barriers in smaller particles.

- Increased reduction extent is achieved with increased radiation heat transfer to the sample surface, irrespective of factors such as reductant reactivity and material layer thickness.

- Future work should include a mathematical model of the reaction system presented in this work. Such a model will provide a method to test the effect of individual possible rate controlling parameters independently from each other: radiation heat transfer, conduction heat transfer within the material layer, gasification rate, reduction rate and devolatilisation rate. The effect of each of these parameters on the overall reaction system productivity can be tested individually in the model by adjusting the model parameters that determine each of these parameters: furnace heating surface temperatures to simulate radiation heat transfer effects, material bed thermal conductivity to simulate conduction heat transfer effects within the material layer, reaction rate constants to simulate the effects of reaction rates for reduction, gasification and devolatilisation.